Check for updates

Recent progress in semiconductor/graphene photocatalysts: synthesis, photocatalytic applications, and challenges

Mahmoud A. Ahmed †* and Ashraf A. Mohamed †

The presence of an increasing number of organic pollutants in water now poses serious risks to both human health and ecological systems. Many of these pollutants are persistent and non-biodegradable. The contamination of fresh water by harmful substances has compelled researchers to develop innovative, efficient, and cost-effective water remediation techniques and materials. Thus, photocatalysis has long been recognized as a promising approach to tackle both environmental remediation and the energy crisis. However, semiconductor photocatalysts frequently suffer from defects such as photo-generated charge carrier recombination, poor visible light response, and slow surface reaction kinetics, which can be remedied by modifications with appropriate co-catalysts. Therefore, graphene and its derivatives have widely been used as supports for semiconductors and photocatalysts due to their distinctive optical, physicochemical, and electrical features. This critical review addresses the current progress in the design and synthesis of graphene/semiconductor photocatalysts, as well as their use in photocatalytic degradation of organic pollutants and hydrogen production. Several influencing parameters are addressed, including pH, photocatalyst loading, initial pollutant concentration, light wavelength, and oxidizing species, all of which could have a significant impact on the rate of organic pollutant's degradation. Furthermore, the recyclability of the catalyst and its photocatalytic activity mechanisms are thoroughly discussed. Numerous case studies are systematically presented. Moreover, future prospects and major challenges are highlighted.

Chemistry Department, Faculty of Science, Ain Shams University, Cairo, 11566, Egypt.
E-mail: mahmoudmhmoud_p@sci.asu.edu.eg
† Both authors contributed equally.

1. Introduction

Freshwater of appropriate quality is critical for public health, whether it is used for industrial, agricultural, drinking, or domestic purposes; however, water pollution is becoming

Mahmoud Adel Ahmed is currently a doctorate student under the supervision of Prof. Ashraf A. Mohamed, in the Department of Chemistry, Faculty of Science, Ain Shams University, Cairo, Egypt. He earned his M. Sc. degree in 2019. He is actively engaged in the research for the past six years and his research focuses on synthesis, characterization, and environmental applications of nanomaterials and their composites. He has been working for Veolia Environmental Services as a service engineer in water desalination and wastewater treatment for 10 years.

Ashraf A. Mohamed is a Professor of environmental analytical chemistry, in the Department of Chemistry, Faculty of Science, Ain Shams University, Cairo, Egypt. He earned his M. Sc. degree in 1991, PhD degree in 1995. He is actively engaged in the research for the past 35 years and his research interests include nano-materials, layered double hydroxides, molecularly imprinted polymers, water treatment and analysis, optical sensors, and paper microfluidics.

a major threat as a result of globalization, urbanization, and anthropogenic activities.[1,2] Water pollution is defined as any change in the biological, physical, or chemical characteristics of water in lakes, rivers, oceans, and/or groundwater. The three most common types of water pollutants are organic pollutants (*e.g.*, hydrocarbons, dyes, pesticides, pharmaceuticals, phenols), biological pollutants (*e.g.*, microorganisms), and inorganic pollutants (*e.g.*, heavy metals).[3–5] An appreciable fraction of dyes contain known carcinogenic moieties such as naphthalene, benzidine, or quinonoid structures.[6,7] Various types of dyes are available commercially, and they are used in various industrial dyeing processes, *e.g.*, in rubber, textile, paper, paint, printing, plastic, pharmaceutical, cosmetics, food, and leather sectors.[6,8] The world consumes over 800 000 tons of organic dyes annually, where approximately 20% of the total dyes production is wasted during various industrial dying processes.[9–11] Effluents resulting from the textile and dyeing industries process usually contain mixtures of dyes, metal ions, and other pollutants, as well as to its elevated levels of biochemical oxygen demand, pH, suspended solids, chemical oxygen demand, salts, and colors.[6] The discharge of these pollutants into bodies of water without proper treatment can have serious consequences, such as toxicity to mammals, fish, and aquatic microorganisms, and can even obstruct the photosynthesis of aquatic plants, resulting in the destruction of the aquatic ecosystem.[12,13] As a result, innovative, cost-effective, recyclable, and environmentally friendly approaches are required to eliminate these dangerous threats. Several approaches have been widely employed in industrial sectors to eliminate organic pollutants, and heavy metals from real wastewater; *e.g.*, reverse osmosis, ion exchange, coagulation–flocculation, ultrafiltration, electrodialysis, adsorption, chemical precipitation, and solvent extraction.[6,14,15] Due to the renewability of solar light, sustainability, and the global energy crisis, photocatalytic process has emerged as a desirable green solution to deal with the worsening environmental problem and energy crisis and through degradation of organic contaminants and generation of hydrogen, respectively.[16,17] With ever-increasing energy consumption that exceeds its supply, the globe is edging closer to a grave energy catastrophe. We take it for granted while always knowing that the energy we consume on a daily basis is finite. Water, oil, gas, and power are all scarce resources. Hydrogen is considered a renewable power resource due to near-zero-emission operation and has great energy density as well as provides high-quality energy services in a wide range of applications.[3,4] As a result, there has recently been a lot of interest in the development of photocatalytic processes based on semiconductors due to their ease of use, high stability, low cost, suitable band positions, and nontoxic nature.[18,19] Furthermore, some semiconductor-based materials can conduct electrons in the presence of light even at room temperature. With incident radiation of proper energy ($h\nu$) that is equal to or greater than the bandgap energy of a photocatalyst, an electron in the valence band (VB) is transferred into the conduction band (CB) level, with the formation of a hole in the VB.[20–22] The excited electron and photogenerated holes play a critical role in photocatalytic degradation of organic

pollutants, as well as solar energy conversions such as solar photovoltaics and hydrogen production.[23–27] However, there are some drawbacks that limit the widespread use of photocatalysts in practical applications; *e.g.*, the high bandgap energy, the poor visible light absorption, and the ease of electron–hole recombination that waste energy as heat and result in poor photocatalytic activity.[28,29] Therefore, several strategies have been used over the last decade to improve the photocatalytic behavior of semiconductor photocatalysts; *e.g.*, by proper textural design, noble metal doping, and tailoring of proper composites. In particular, several studies have incorporated graphene-based materials with semiconductors to improve their photocatalytic performance. Graphene is a single 2D nanosheet with sp² hybridization that has a honeycomb-like structure, zero bandgap energy, possessing distinctive electrical features such as ballistic electronic transport, massless fermions, and extremely high electron mobility (200 000 cm² V⁻¹ s⁻¹). Moreover, graphene has a large surface area (2630 m² g⁻¹), a highly flexible structure, high thermal conductivity ($\approx$5000 W m⁻¹ K⁻¹), and high transparency (optical transmittance is 97.7%).[6,8,30–33] Graphene is hydrophobic and chemically inert due to the absence of undesirable functional groups. Reduced graphene oxide (rGO) and graphene oxide (GO) are two common counterparts of graphene. GO is commonly synthesized by the oxidation of pristine graphite. GO contains an abundance of groups on both sides of its sheet, namely hydroxyl epoxy on the basal plane, and carboxyl and carbonyl at the layer boundaries, which in turn enables GO to form stable suspensions in solutions, and also work as sites for semiconductors nucleation and growth. However, an excess of groups in non-conducting σ states may lead to the insulation of GO, which reduces the separation and transport of charge carriers.[34–36] The number of groups generated on the GO layers depends on the type of used graphite and the oxidation conditions. The miniature form of GO is rGO, which can be made from chemical/thermal reduction or direct growth of GO. Thus, rGO has fewer surface groups and an excessive amount of defects, which makes it more chemically stable and has higher electrical conductivity compared to its parent GO. Due to these distinctive features, graphene and its counterparts (GO and rGO) have drawn great interest in photocatalytic applications.[37,38] The scientific works published on graphene-based photocatalysis over the period 2006 to 2022_11 are illustrated in Fig. 1. A total of 4630 publications have been incorporated into the Scopus database under the keywords "photocatalysis and graphene". These papers have been categorized as; 86% journal articles, 5% conference papers and book chapters, and 8% reviews, this illustrates the importance of reviews devoted to the topic.

Herein, we provide a critical and comprehensive review of the use of graphene-based semiconductors in photocatalytic degradation of organic pollutants and hydrogen production. The methods of synthesis, physicochemical characterization, and photocatalytic activity are thoroughly reviewed, in a chronological order, with numerous representative examples. The operating parameter, the recyclability, and the mechanisms of the photocatalytic processes are also discussed. In addition, we attempted to present challenges for improving the
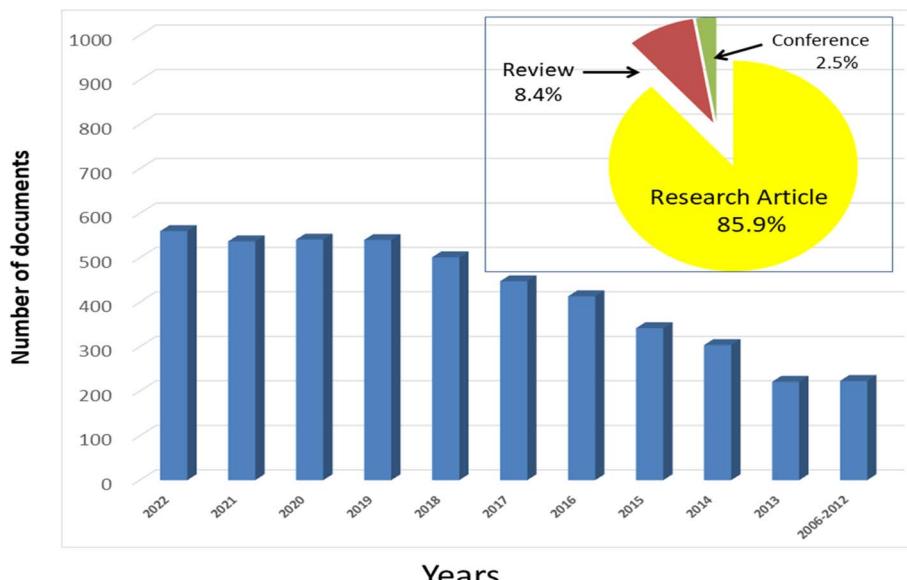
Fig. 1 Number of publications in Scopus database reporting graphene/semiconductors materials for photocatalytic reaction (keywords: graphene AND photocatalysis).

photocatalytic performance of graphene-based semiconductors for industrial applications. We believe this review will benefit researchers in the fields of photocatalysis, graphene and semiconductors-based nanomaterials.

2. Preparation of graphene/semiconductors composites

Various semiconductor materials have been utilized for the production of graphene-based photocatalysts. These include metal oxides, metal sulfides, silver/silver halides, salts, and metal-free polymers like graphitic carbon nitride, as well as others.[39–41] There are two basic methods of preparation: (1) *in situ* crystallization, in which nanocrystals form and grow on graphene-based material surfaces, and (2) *ex situ* crystallization, in which pre-fabricated nanomaterials are mixed with graphene-based material surfaces.[42] The *in situ* method results in a homogeneous distribution of semiconductors on 2D nanosheets of the graphene material; moreover, the functional groups present on GO can be used to control the crystallinity, size, and morphology of the *in situ* grown semiconductor crystals. In addition, the direct contact of graphene sheets with semiconductor nanoparticles promotes the electron's transfer among them.[43,44] On the other hand, the *ex situ* hybridization approach is good at overcoming any incompatibility between compounds and enables to co-assembly of nanoparticles of various textures, sizes, and shapes on sheets of graphene or its derivatives.[45,46] However, the *ex situ* approach suffers from non-uniform distribution and low density of semiconductors on the surface of graphene or its derivatives.[46,47] There are several methods utilized to synthesize semiconductors/graphene photocatalysis including solvo/hydrothermal, microwave-assisted deposition, sol–gel, and solution mixing.[48–51]

Hydro/solvothermal methods are widely utilized to synthesize graphene/semiconductor photocatalysts due to its low cost, simplicity, effectiveness, environmental friendliness and the uniform distribution of semiconductor nanomaterials on graphene sheets' surfaces.[52] However, these methods are very sensitive to the operating conditions such as temperature, pH, and time. Often methanol, ethanol or water is used as a solvent and the nanoparticles are grown under high pressure and temperature.[7] For example, ZnS/graphene nanoplatelets were synthesized by a solvothermal route, wherein a mixture of graphene nanoplatelets and zinc acetate in ethylene glycol were ultrasonicated for an hour, and sodium sulfide solution was added into the mixture that was then transferred into an autoclave and heated to 1600 °C for 15 h.[53] The obtained ZnS/graphene nanoplatelets composite was then characterized by SEM, Raman, AFM, XRD, and DRS studies.[53] Further, a series of Cu_2O–rGO was synthesized through solvothermal method for the photocatalytic degradation Rhodamine B dye.[54] The SEM and FTIR data confirmed the reduction of GO and the successful fabrication of Cu_2O/rGO_x composites with various wt% of rGO to Cu_2O, where x (0, 0.05, 0.1, 0.2 and 0.5 wt%), respectively; Fig. 2a and c. Moreover, the BET analysis showed that all composites have greater surface areas than pare Cu_2O (Fig. 2d).[54] Further, rGO/Fe_3O_4 nanocomposites with various mass ratios were synthesized through the solvothermal method, where SEM analysis revealed that Fe_3O_4 particles, with average diameter in the range of 131–237 nm, were densely distributed on both sides of rGO sheets preventing the restacking of rGO sheets.[55] Moreover, rGO/TiO_2 nanocomposites with various ratios of GO were synthesized *via* solvothermal method.[56] On the other hand, a graphene/CdS composite photocatalyst for the efficient H_2-production was fabricated through a solvothermal route where CdS uniformly decorated the graphene sheets.[57] The observed high
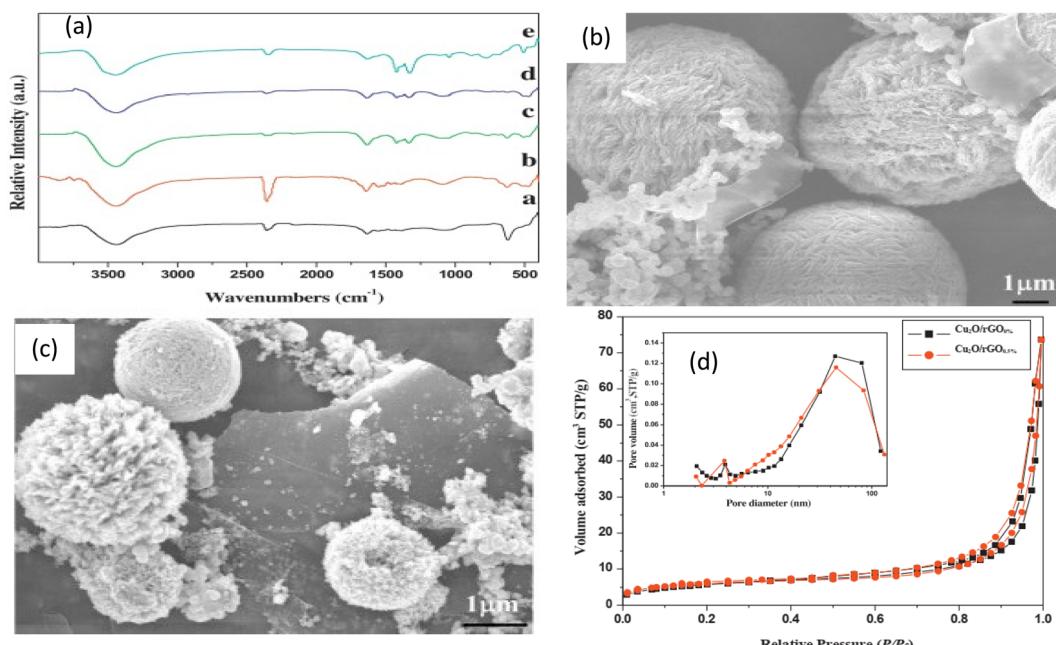
Fig. 2 (a) FT-IR spectra of as-prepared $Cu_2O/rGO_{x\%}$ samples with various wt% of rGO, (b and c) FESEM image of Cu_2O/rGO 0.05, and 0.5% (wt%), respectively, and (d) N_2-adsorption isotherms of $Cu_2O/rGO_{0\%}$ and $Cu_2O/rGO_{0.5\%}$ (wt) reprinted with permission from ref. 54. Copyright 2022 Elsevier.

photocatalytic H_2-production activity was attributed predominantly to the presence of graphene that served as an electron collector and transporter to efficiently lengthen the lifetime of the photogenerated charge carriers from CdS nanoparticles.[57]

The sol–gel method is a multistep wet chemical process for the engineering and synthesis of photocatalysts that involves sequentially hydrolyzing molecular precursors such as metal chlorides, metal alkoxides, or organometallic compounds followed by instant polycondensation to form a sol–gel.[58] This method has several advantages, including low cost, high product homogeneity and purity, ease of manufacture, and low procedure temperatures. Furthermore, surface groups in rGO/GO serve as semiconductor nucleation sites for attachment with the produced metal oxides. Thus, rGO/ZnO with various mass ratios of rGO was synthesized through the sol–gel method and was used to generate a photocurrent. The TEM images revealed a 19 ± 2 nm particle size of ZnO dispersed on the surfaces of rGO sheets; whereas HRTEM images revealed that the weight ratio of rGO affected the crystallinity of the NPs.[59] Further, GO/TiO_2 thin films were prepared through a sol–gel route where GO markedly enhanced the photocatalytic activity of TiO_2.[50] Moreover, mesoporous $G/TiO_2/SiO_2$ nanocomposites were synthesized by the direct sol–gel co-condensation combined with hydrothermal treatment, where graphene similarly exerted a pronounced enhancement of the photocatalytic activity of TiO_2.[60] Further, rGO/TiO_2 hybrid nanocomposites with various rGO ratios were synthesized by sol–gel route followed by calcination and were applied to photocatalytic hydrogen production; where, a 0.25 wt% rGO gave 10 fold enhancement of the photocatalytic activity of bare TiO_2, and

thus suggested rGO as a competitive cocatalyst to replace noble metals cocatalysts.[61]

Microwave irradiation has recently been regarded as a promising tool for the preparation of a wide range of nanomaterials, including bimetallic alloys, metal oxides, semiconductors, and organic compounds, with controlled shape and size and without the need for high pressure or high temperature. Crystalline growth can be controlled during this process by varying the concentrations of different surfactants and the time of the process. Thus, TiO_2/graphene nanocomposite was synthesized through microwave-assisted method that offered a uniform coating and excellent interactions between graphene sheets and TiO_2 semiconductor.[62] Further, GO/ZnO nanostructures of various ZnO dimensions (3D, 2D and 1D) were prepared through the microwave exfoliation synthesis under different irradiation times; with the schematic procedure for the preparation of various GO–ZnO nanostructures as shown in Fig. 3.[63] Moreover, graphene/ZnS nanocomposite was synthesized, in aqueous medium, by microwave-assisted approach during which the GO was converted to graphene; where after photoluminescence studied revealed an electron transfer between graphene nanosheets and ZnS.[64]

Ultrasonic synthesis involves the mixing of graphene or its derivatives with the semiconductor precursors under ultrasonic agitation and mixing where the semiconductors uniformly distribute themselves on surface of graphene sheets and interconnect with them when the liquid is evaporated, to produce the photocatalyst composite. For instance, ZnO/rGO composite was synthesized through a simple ultrasound mixing approach and characterized by various techniques, Fig. 4a–e.[65] The synthesized ZnO/rGO composite had a band gap of less than
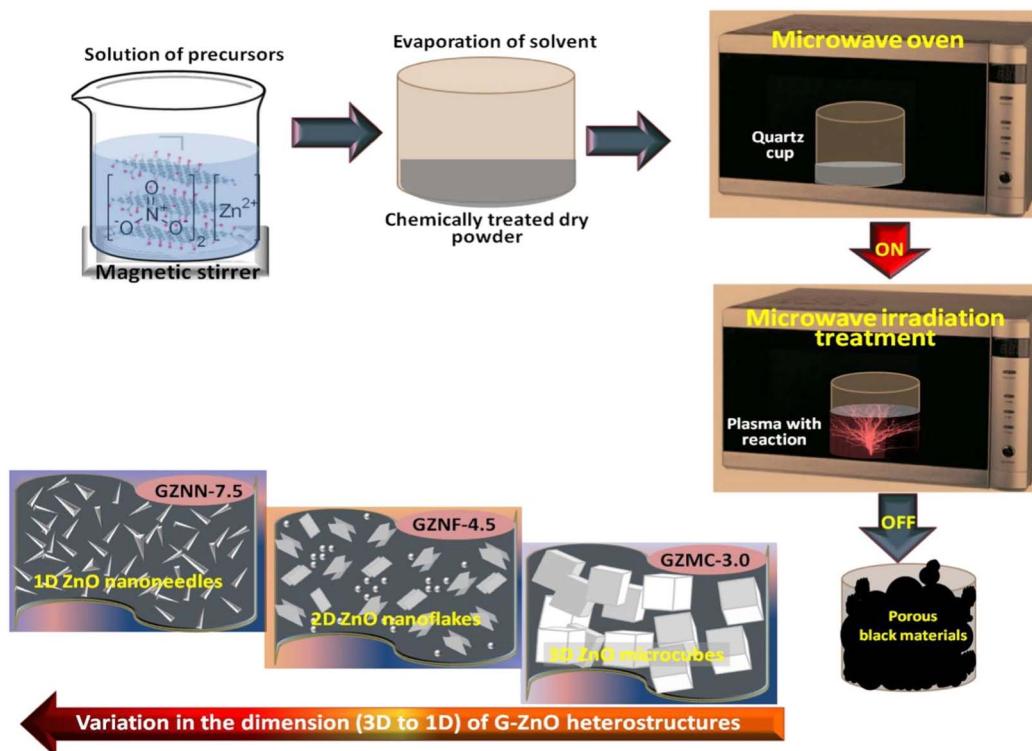
Fig. 3 Schematic diagram of microwave assisted synthesis and formation of different GO–ZnO heterostructures including: GO-3D-ZnO microcubes (GZMC-3.0), GO-2D-ZnO nanoflakes (GZNF-4.5) and GO-1D-ZnO nanoneedles (GZNN-7.5) with various microwave heating times of 3.0, 4.5, 7.5 min, respectively reprinted with permission from ref. 63. Copyright 2022 Elsevier.

3.03 eV, compared to 3.13 eV for the pure ZnO (Fig. 5c) and FESEM images (Fig. 4d and e) showed the ZnO densely decorating the surfaces of the rGO sheets.[65] Moreover, a graphene/ TiO$_2$ photocatalyst was synthesized by ultrasonically mixing graphene oxide with titanium tetrachloride (TiCl$_4$) in an ethanol–water, followed by reducing by hydrazine.[66] Further,
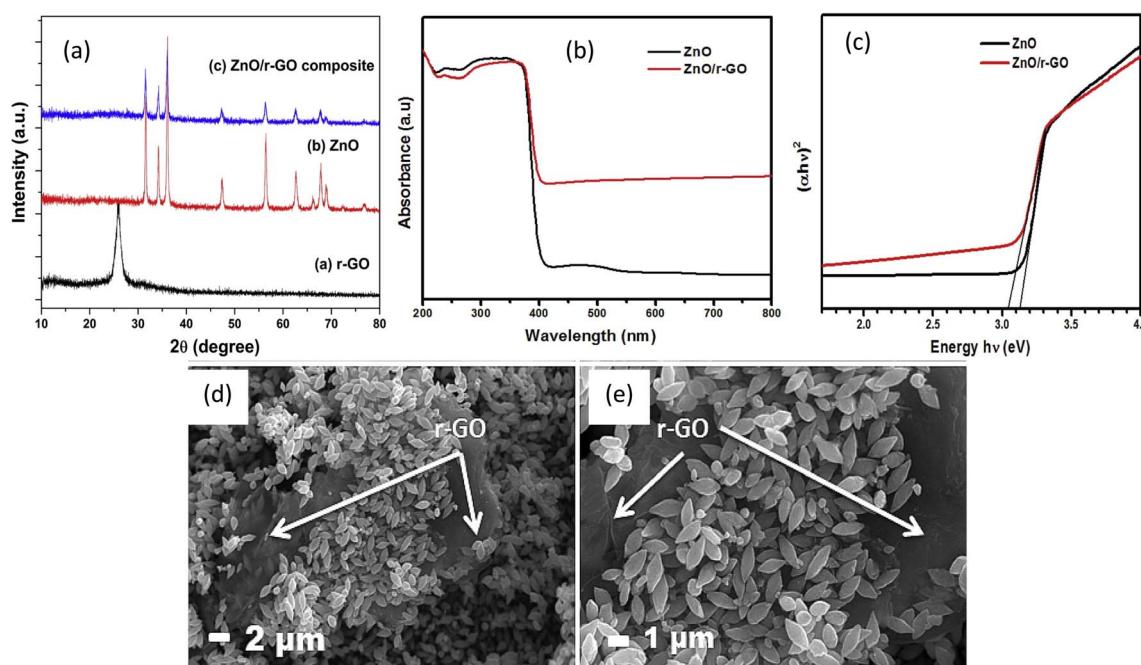

Fig. 4 (a) XRD patterns, (b) UV absorption spectra, (c) Tauc plot, and (d, e) FESM of synthesized samples reprinted with permission from ref. 65. Copyright 2022 Elsevier.
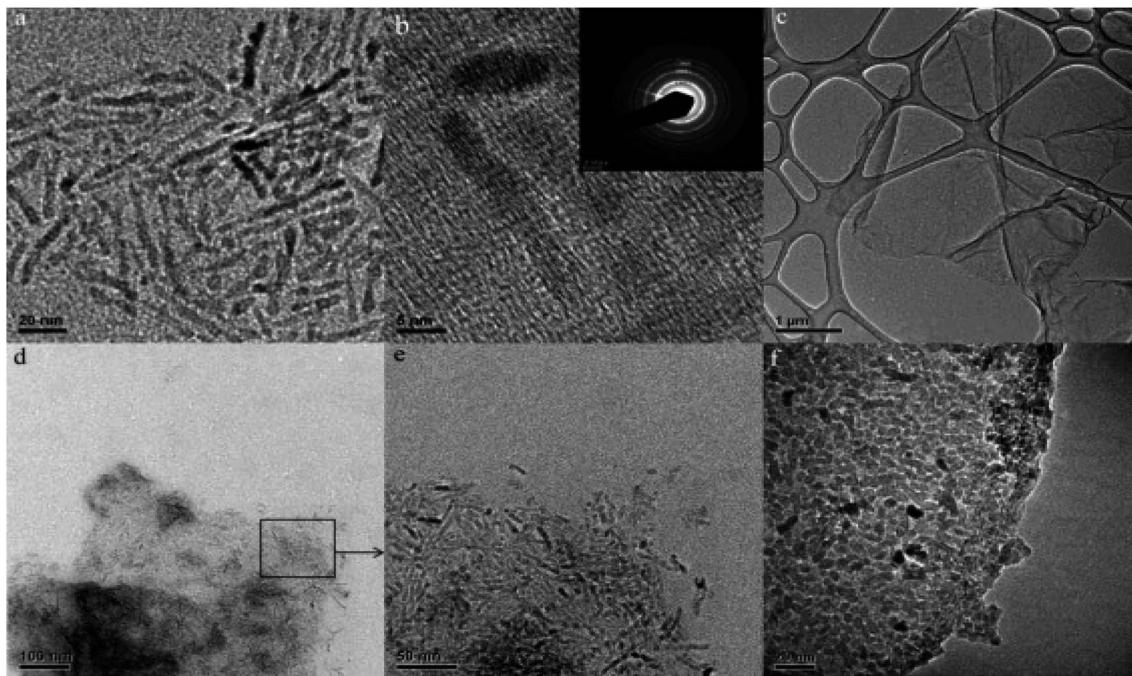
Fig. 5 TEM images of (a) TiO$_2$ NRs; (b) HRTEM and SEAD of TiO$_2$ NRs; (c) GO; (d) TiO$_2$ NRs anchored on GO sheets; (e) enlargement of image d; and (f) TiO$_2$ NPs anchored on GO sheets reprinted with permission from ref. 67. Copyright 2022 Elsevier.

two composites of TiO$_2$ nanoparticles/GO and TiO$_2$ nanorods/GO were synthesized by ultrasonic mixing of suspensions of GO and TiO$_2$ nanoparticles or nanorods.[67] The HRTEM images of TiO$_2$ nanorods and both composites was illustrated in (Fig. 5a and f).[67]

3. Mechanisms of photocatalysis

Semiconductors usually have a high photosensitivity and crystallinity, a large bandgap, and a low absorption capacity. However, when combined with graphene or its derivatives, semiconductors demonstrated improved photocatalytic activity *via* variety of mechanisms:

3.1 Increasing light absorption harvesting

The fabrication of composites of graphene-based materials and semiconductors, under optimum conditions, usually involve bond formations between the surfaces of graphene materials and the semiconductor that can enhance light harvesting by increasing the light absorption intensity and edge. For instance, diffuse reflectance spectrometric (DRS) analysis showed increased light absorption and edge of ZnS/G composite in visible region compared to pure ZnS due to the black color of graphene, and the band gap decreased from 3.58 eV for ZnS to 3.27 eV for the ZnS/G nanocomposite, Fig. 6a–d.[53] Similarly, introducing rGO into ZnO improved its photocatalytic activity by enhancing the light absorption range and intensity.[68] Furthermore, the synthesized ZnS/rGO photocatalyst, with various ratios of rGO, exhibited a red shift in the absorption edge of the synthesized composites while also improving its light-harvesting capability.[69]

3.2 Enhancement the adsorptive ability of semiconductors

Adsorption of pollutants on the photocatalysis plays an important role in the photo-degradation process because this process mainly occurs on the surface of the photocatalysts. Graphene has a high surface area and an abundance of π electrons, whereas GO and rGO have plenty of –C=O, –C–O–C, –C–OH, –COOH, among other fruitful functional groups that lead to improved adsorption ability of photocatalysts towards various pollutants by increasing active adsorption sites *via* electrostatic interactions, hydrogen bonding, and π–π, n–π and van der Waals interaction mechanisms. However, an excess amount of the graphene material can lead to an increased collisions holes and electrons and thus dramatically reduce the catalytic efficiency of the composites. As a result, the ratio of graphene material plays a critical role in the performance of synthesized composites and must be carefully optimized. For example, the presence of GO improved the removal efficiency of MB by rGO/TiO$_2$ because of the abundance of active removal sites, which extremely enhanced the π–π interaction between the graphitic skeleton of rGO and aromatic rings of methylene blue (MB), in addition to the electrostatic interaction between the residual functional groups of rGO and cationic centers of MB molecules.[56] Similarly, the incorporation of rGO onto CuI enhanced the overall removal of Rhodamine-B dye.[70]

3.3 Transport of excited electrons from synthesized semiconductors

A semiconductor has an electron-occupied valence band (VB) and an unoccupied conduction band (CB), and the difference between them is known as the band gap. When light with
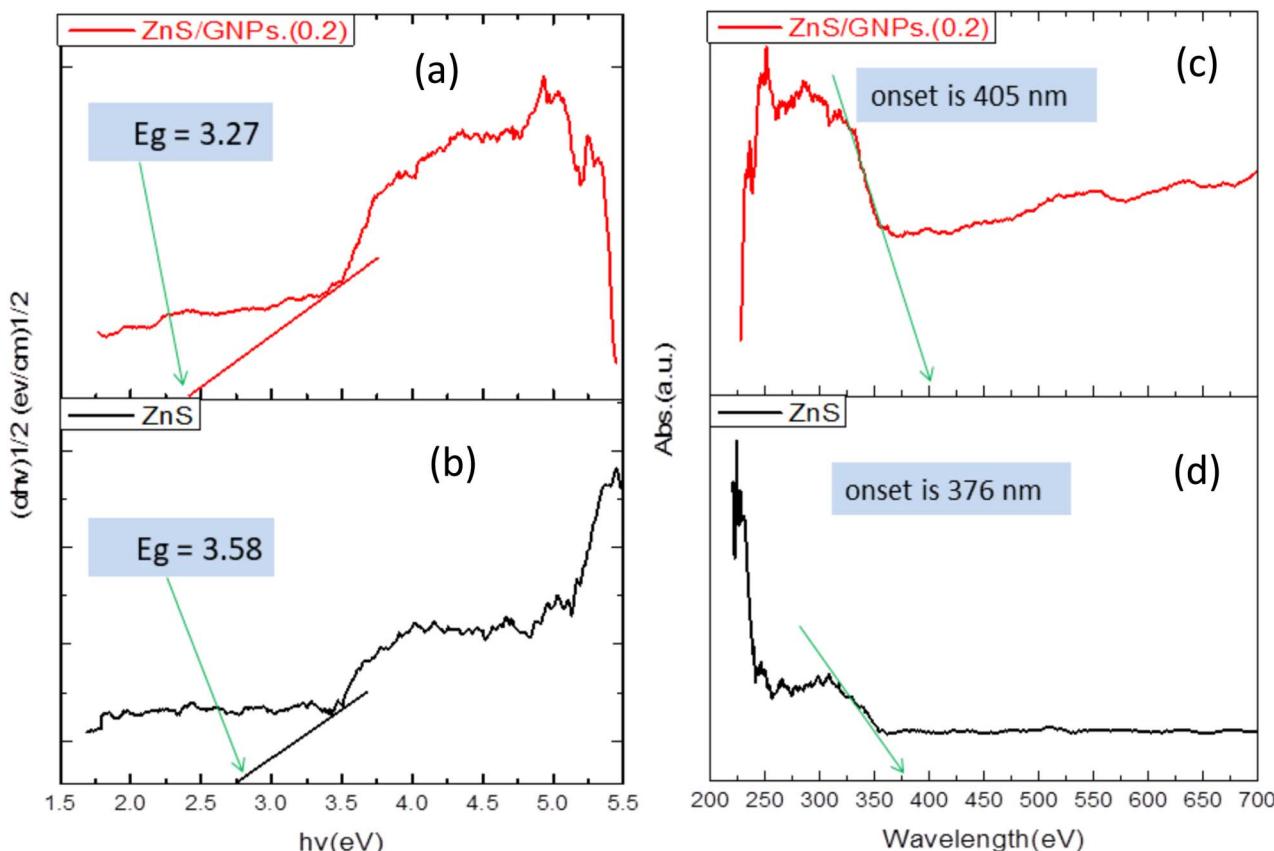
Fig. 6   Band gaps of ZnS/G NPs (a) and ZnS (b); and diffuse reflectance spectra of ZnS/G NPs (c) and ZnS (d), respectively.[53]

energy greater than a semiconductor's band gap (E_g) is incident on it, electrons in the VB are transported to the CB, resulting in the formation of positive holes (h^+) in the VB and photo-excited electrons (e^-). The suffering of semiconductor photocatalysts is caused by the rapid recombination of e^- and h^+, in which photogenerated electrons recombine within 10 nanoseconds. Photocatalytic processes are severely limited in their efficiency due to the rapid recombination of positive holes and excited electrons. Graphene-based materials are used as electronic accumulators, which can transport electrons over their 2D structures and effectively promote the separation of photogenerated electron–hole pairs while inhibiting electron–hole recombination. The Fermi level of graphene materials is typically lower than the CB of most semiconductors, allowing excited electrons to be transported to graphene or its derivatives. The increased electron path length and decreased recombination of holes and photogenerated electrons improve the graphenes/semiconductor photocatalytic efficiency. For example, rGO enhanced the photocatalytic efficiency of WO_3, where DRS and PL optical measurements; Fig. 7a, revealed that the recombination of electron–hole pair of WO_3 photocatalyst was highly prohibited after rGO incorporation, at the four different rGO wt% studied.[71] Further, incorporation of graphene into In_2S_3 significantly improved the photoelectrochemical characteristics of pure In_2S_3, as shown in Fig. 7b.[72] The photocurrent density of graphene/In_2S_3 was the

highest, demonstrating that the separation and transfer of photogenerated electron–hole pair had been greatly improved over bare In_2S_3.[72] Moreover, CB electrons of the NiS semiconductor were transferred to the rGO sheets of rGO/NiS composite reducing the extent of electron–hole recombination in NiS and thus leading to enhanced photocatalytic activity of the rGO/NiS catalyst.[73] The general mechanisms of photocatalytic activity of semiconductor–graphene based binary and ternary composites are illustrated in Fig. 7c and d, respectively.[27,74] For the binary system (Fig. 7c) when the radiation source hits the photocatalyst, photo-excited electrons (e^-) are transferred from VB to CB in the PC and leaves holes (h^+) behind. Subsequently, the excited electron moves from the conduction band to the graphene sheets which results in enhanced charge separation. Then, the excited electron are react with oxygen dissolved in system or adsorbed onto the surface of photocatalyst to produce superoxide radical anion ($^{\bullet}O_2^-$), which then reacts with water producing hydroxyl radicals. In addition, the holes react with OH^- ions or water to generate the powerful oxidant, hydroxyl radicals. These radicals enrich the nanocomposite surfaces, protracted by the more stable carbon free radicals derived from GO/RGO nanosheets and effectively degrades the organic pollutants. In the ternary system, Fig. 7d, extra steps occur; namely, the incident light leads to the formation of electron/hole pairs in both photocatalysts (PC-I & PC-II). The interface between semiconductors
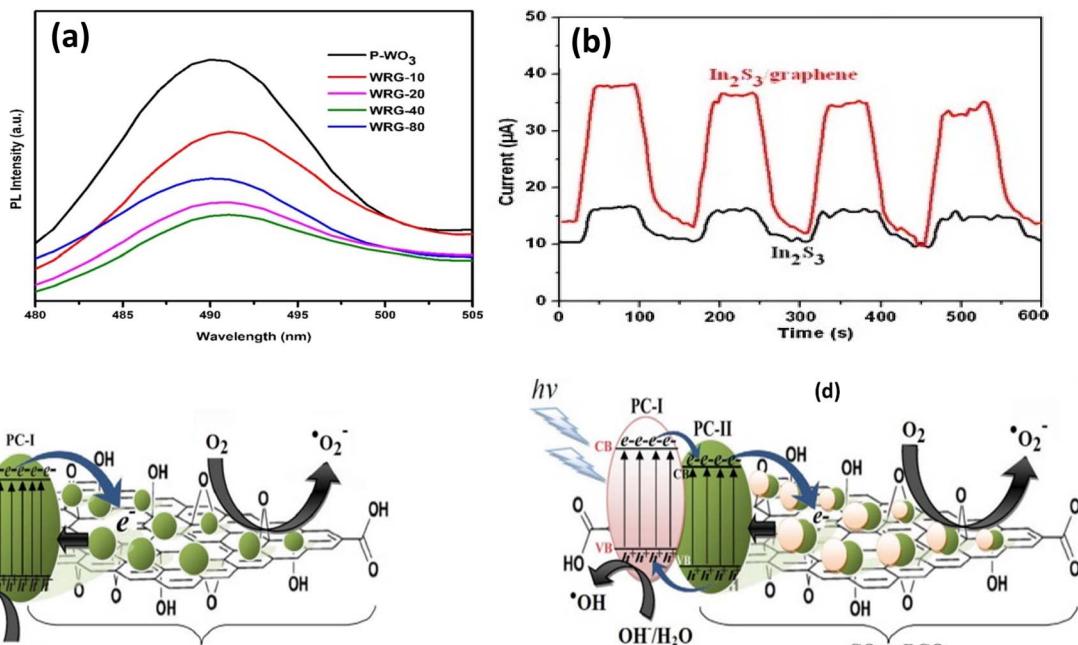
Fig. 7 (a) Photoluminescence spectra of WO_3 and WO_3/rGO composites reprinted with permission from ref. 71, (b) transient photocurrent response of In_2S_3 and $In_2S_3/graphene$ composites under visible light irradiation reprinted with permission from ref. 72, (c) mechanism of radicals generation using photocatalyst (PC)-doped GO/RGO binary nanocomposites, and (d) mechanism of radicals generation using dual-semi-conductor (PC1 and PC2)-doped GO/RGO ternary nanocomposites reprinted with permission from ref. 27. Copyright 2022 Elsevier.

materials (PC-I & PC-II) could enhance the charge separation. Commonly, excited electrons from the higher potential CB of PC-I is transferred to the lower potential CB of PC-II, and then to the graphene material sheets that enhance charge separations and hinder the electron–hole recombination. Then, the formed photoexcited electrons and holes react with oxygen and water to finally produce the highly reactive hydroxyl radicals responsible for organic pollutants degradation.

As a result, the overall improved photocatalytic efficiency of graphene-based photocatalysts can be attributed to better electron–hole pair separation, easier charge transportation ability, improved adsorption ability, reduced band gap energy, and improved visible light harvesting.

4. Photocatalytic applications

4.1 Degradation of organic pollutants

The discharge of a significant amount of contaminated water into the environment, which contains dyes, pesticides, pharmaceuticals, and phenols among other organic pollutants, is one of the results of progress and industrial diversification around the world. Photocatalysis is the most effective and easy method for the remediation and elimination of organic pollutants because of its comprehensive contaminant deconstruction ability. Here, we discussed some GO-supported semiconductor composites for the elimination of organic pollutants. For example, GO/ZnO hybrid layers was synthesized and exhibited higher photocatalytic performance over pure GO or ZnO under visible and UV-light irradiation. The improvement in the photocatalytic performance of the hybrid was attributed

to the role of GO in the separation and transport of the excited electron and positive hole.[75] Further, incorporation of 5% rGO into TiO_2 for the degradation MB dye gave superior photodegradation performance with about 86% removal of MB dye in 90 min compared to 28% removal for pristine TiO_2 in the same time, following PFO kinetics.[76] Moreover, the UV-vis spectra of MB dye after the photodegradation in the presence of $MnFe_2O_4$ and $MnFe_2O_4/rGO$ are displayed in Fig. 8a and b, respectively.[77] Pristine $MnFe_2O_4$, took 290 minutes to eliminate 84% of the dye; while $MnFe_2O_4/rGO$ required 60 min to eliminate 97% of the dye, showing the enhanced catalytic efficiency upon the incorporation of rGO into $MnFe_2O_4$ with the resultant delay in the electron–hole recombination rate of the catalyst.[77] The photocatalytic decomposition of Rhodamine B (RhB) dye by TiO_2 NPs, TiO_2 nanowires (TNWs), GO/TNW and its reduced composites RTNW and R(GO/TNW) samples were examined, Fig. 9.[78] The degradation performance enhanced monotonically from TiO_2 NPs to TNWs and its GO/TNW composites; moreover, it was enhanced from RTNWs to R(GO/TNW)s as well, demonstrating an overall improvement in pore size and specific surface areas in nanowires and their composite after coupling with GO.[78] Moreover, several works were carried on for the synthesis of significantly efficient graphene-based heterostructure ternary composites. For example, $GO/Fe_2O_3/WO_3$ composite was synthesized and utilized for the photodegradation of crystal violet and MB dyes under visible light irradiation. The photocatalytic activity for eliminating dyes was found to be significantly enhanced with the heterocomposite as compared to pristine WO_3 and Fe_2O_3 particles or composite of Fe_2O_3/WO_3, WO_3/GO and Fe_2O_3/GO.[79] The improvement in the
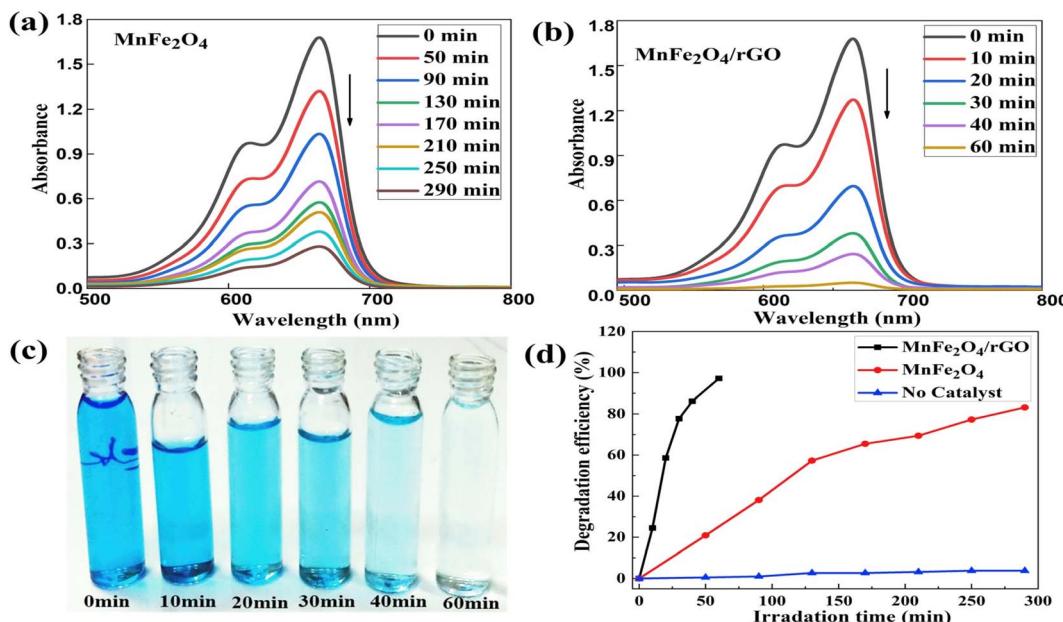
Fig. 8 Degradation of MB over (a) $MnFe_2O_4$ nanoparticles, and (b) $MnFe_2O_4$/rGO, (c) change in color of the MB solution in presence of $MnFe_2O_4$/rGO, (d) the photocatalytic degradation efficiency of MB dye in the absence (blue) and presence of photocatalysts: $MnFe_2O_4$ (red), $MnFe_2O_4$/rGO (black) at different UV irradiation times reprinted with permission from ref. 77. Copyright 2022 Elsevier.

photocatalytic activity of the ternary Fe_2O_3/GO/WO_3 photo-catalyst is attributed to Z-Scheme in which the excited electrons in the CB of WO_3 (photosystem I) transferred over graphene oxide as mediator and recombined with the positive holes in the VB of Fe_2O_3 (photosystem II). Hence, the hole–electron pair recombination can be delayed in both systems.[79] Further, Fe_3O_4@CuO-rGO ternary photocatalyst was synthesized by

a hydrothermal method and was applied to MB dye photo-degradation.[80] The as-synthesized Fe_3O_4@CuO-rGO photo-catalyst has a broad-visible illumination adsorption domain and improved charge separation compared to pristine CuO or Fe_3O_4@CuO composite, as well as improved photocatalytic activity toward MB dye degradation under visible light illumi-nation surpassing those of CuO, Fe_3O_4, CuO–rGO, Fe_3O_4–rGO,
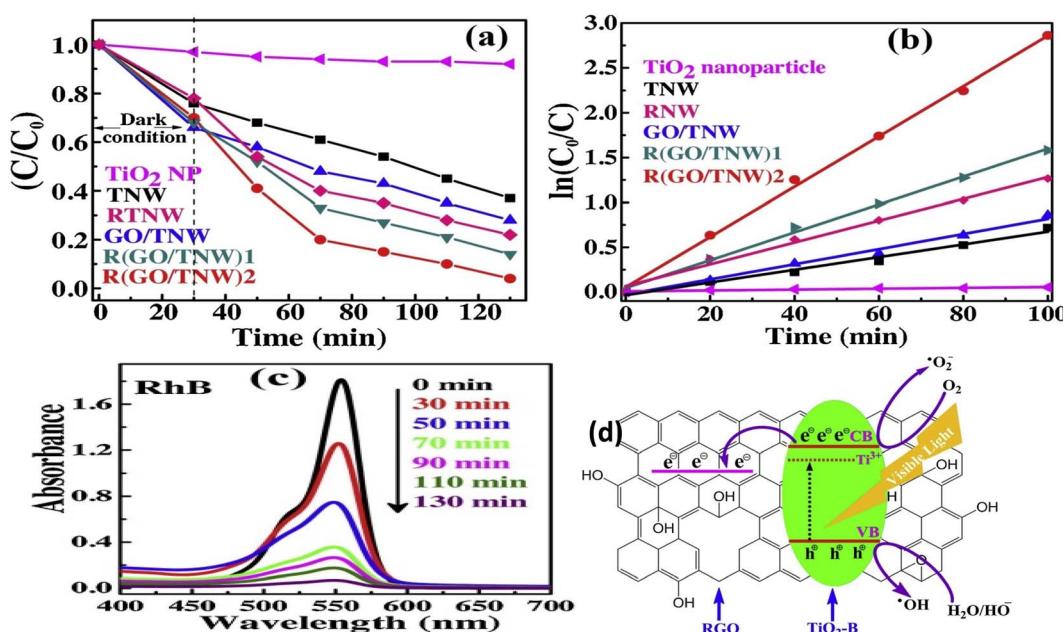
Fig. 9 (a) Plot of (C/C_0) *versus* time for degradation of RhB in the visible light, (b) kinetics of photodecomposition of the prepared samples, and (c) the absorption spectra of RhB under visible light irradiation catalyzed by R(GO/TNW)$_2$ composite, and (d) schematic diagram elucidating the mechanism of photocatalytic activity of R(GO/TNW)$_2$ reprinted with permission from ref. 78. Copyright 2022 Elsevier.

Table 1 Photocatalytic degradation performance of various GO based binary photocatalysts[a]

Photocatalyst composite	Pollutants	Light source	Initial concentration	Catalyst dose	Irradiation time (min)	Degradation (%)	Ref.
TiO_2/graphene	MO	300 W Xe-lamp	10 ppm	50 mg	210	100	111
AgI/RGO (0.4 wt%)	RhB		10 ppm	100 mg	70	96	112
$CoFe_2O_4$–graphene	AB	Visible light	20 ppm	10 mg	240	66	113
$BiVO_4$–graphene	RhB	Visible light	20 ppm	50 mg	300	99	114
Graphene–CdS	RhB	Visible light	1.0×10^{-5} M	20 mg	80	95	115
PANI/rGO (rGO-5% wt.)	MG	Visible light	1.7×10^{-5} M	10 mg	15	99.68	116
	RhB		1.7×10^{-5} M		30	99.35	
	CR		1.7×10^{-5} M		45	98.73	
Ag_3PO_4@RGO (4 wt%)	AB25		18 μmol L^{-1}	0.75 g L^{-1}	60	100	117
WO_3/graphene	MB	400 W lamp	10 ppm	2.0 mg	300	80	118
TiO_2/GO	MB	Visible light	100 ppm	100 mg	300	67.45	119
	MR		100 ppm	100 mg	300	30.56	
	CR		100 ppm	100 mg	300	35.79	
TiO_2	MB		100 ppm	100 mg	300	24.6	
	MR		100 ppm	100 mg	300	16.68	
	CR		100 ppm	100 mg	300	17.78	
SnO_2–rGO	*p*-Hitropophenol	UV lamp, 254 nm, 8 W	200 ppm	50 mg	90.0	95.6	120
Fe_3O_4/rGO	Phenol	Visible light	10 ppm	1000 mg	120	76	121
TiO_2/Graphene	Phenol	Visible light	50 ppm	1000 mg	360	68	122
$Ce_2Zr_2O_7$/rGO	Ciprofloxacin	250 W Hg- lamp	10 ppm	100 mg	60	89	123
NiFe-LDH/rGO	Moxifloxacin	10 W LED lamp	20 ppm	100 mg	60	63	124
Ag_3PO_4/graphene hydrogel	BPA	Visible light, 250 W, metal halide lamp	10 ppm	150 mg	12	100	125
WO_3@RGO	Phenol	Simulated solar light	10 ppm	1000 mg	240	30	126
$ZnSnO_3$/rGO	Metronidazole	500 W U-shaped Xe lamp	5 ppm	100 mg	180	73	127
CoO@GR	TBBPA	350 W Xe-lamp	10 ppm	1.5 mg	120	69	128
$BiVO_4$/rGO aerogel	HCHO	UV light, 150 W, Xe-lamp	50 ppm	50	15	60	129

[a] PANI/rGO, polyaniline/reduced graphene oxide composite; BG, Brilliant green; NCR, nickel/copper oxide/reduced graphene oxide; MG, malachite green; RhB, Rhodamine B; MB; methylene blue; MR, methyl red; CR, Congo red; T0.05–100/Dia-GO, titanium dioxide/diazonium/graphene oxide; (PVA/PAAc)–RGO–TiO, polyvinyl alcohol/acrylic polyvinyl alcohol/reduced graphene oxide/titanium dioxide; DB71, direct blue 71 dye; MO, Methyl orange; WO_3/graphene, tungsten trioxide nanorods–graphene nanostructure, AB25, Acid Blue 25; AgI/RGO, silver iodide/reduced graphene oxide; AB-BL, active black BL-G, AB, Acid Blue; AY, Acid Yellow; AR, Acid Red; RB, Reactive Blue, RY, Reactive Yellow; RR, Reactive Red; TBBPA, tetrabromobisphenol; BPA, bisphenol; HCHO, gaseous formaldehyde.

Fe_3O_4@CuO, and Fe_3O_4/CuO–RGO catalysts.[80] Tables 1 and 2 illustrate some examples of semiconductor/graphene-based binary and ternary composites used in the photocatalytic degradation of organic pollutants including for example dyes, pharmaceuticals, pesticides, and phenols.

4.1.1 Effect of operating factors. Photocatalytic degradation of organic pollutants is affected by numerous operating conditions, such as the photocatalyst mass, temperature, pH, oxidizing species, initial concentration of pollutant, and irradiation light intensity, wavelength and time, as shown in Fig. 10.[81]

4.1.1.1 Effect of pH. The pH of the medium greatly affects the photocatalyst efficacy as it affects the photogenerated electron–hole pair separation process and the sorption behavior of the semiconductor photocatalyst. The point of zero charge (pzc) of a synthesized photocatalyst mainly depends on the pH of the medium and consequently affects the adsorption behavior towards anionic and cationic pollutants. Moreover, the pH of the medium controls the predominant oxidation species, whereby at higher and lower pH levels, hydroxyl radicals and holes were found to be the most essential oxidation species.[82]

Therefore, determining the ideal pH level is an important step that might affect the photocatalytic process. For instance, the photodegradation efficiency of Orange G dye over GO–TiO_2 and its heteroatom doped variant rGO(NS)–TiO_2 photocatalysts was greatly affected by the medium pH.[83] At low pH values, the surface of the catalyst becomes positively charged that facilitates its attraction with the negatively charged dye molecules; however, at higher pH values the photocatalytic activity was reduced. In another study, MB dye photo degradation improved with raising the pH value due to the increased attraction between the cationic dye and ZnO/graphene/TiO_2 photocatalyst (pH_{pzc} = 6.4); however, at pH > 11.0, OH^- competes with the photocatalyst in attracting the cationic MB molecules resulting in lower decomposition efficiency, Fig. 11a.[84] Further, the photocatalytic degradation of Amido black dye over rGO–NiS was more efficient at neutral pH values.[73] On the other hand, the increased degradation of MO–RhB dyes mixture over CuS–ZnS–G in alkaline (pH 10.38) and acid media (pH 4.45) reflected the role H^+ and OH^- ions in the dye degradation.[85] At acidic conditions, more $H^•$ radicals are formed due to the interaction of H^+ ions with electrons present in graphene layers resulting in

View Article Online

Review   RSC Advances

Table 2 Photocatalytic degradation performance of various GO based ternary photocatalysts[a]

Photocatalyst composite	Pollutants	Light source	Initial conc.	Catalyst dose	Irradiation time (min)	Degradation (%)	Ref.
g-C_3N_4/RGO/WO_3	Ciprofloxacin	Xe-short arc lamp	20 ppm	10 mg	180	85	130
BiOI/Fe_3O_4@GO	2,4-DNP	35 W LED lamp	129 PPM	50 mg	100	100	131
C_3N_4@$MnFe_2O_4$-G	Metronidazole	300 W Xe lamp	20 ppm	100 mg	60	78	132
rGO/SiO_2/ZrO_2	BPA	Metal halide lamps (400 W, $\lambda = 400$ nm)	10 ppm	350 mg	90	87	133
Fe_3O_4@TiO_2-GO	Enrofloxacin	500 W Xe lamp	2 ppm	400 mg	240	96	134
NiAl LDH/Fe_3O_4-rGO	Ciprofloxacin	500 W Xe lamp	10 ppm	250 mg	150	91	135
TiO_2/Gr/30 PW	Phenol	Visible light	50 ppm	1000 mg	360	91	122
Ag–Cu_2O/rGO	Phenol	300 W Xe lamp	10 ppm	50 mg	210	97	136
PANI-TiO_2/rGO hydrogel	BPA	UV, 500 W, Hg lamp	40 ppm	20 mg	100	60	137
$MgFe_2O_4$–TiO_2NPs@GO	MB	Hg-lamp (125 Watt)	50	0.5 g L^{-1}	120	99	138
$BiVO_4$/$BiPO_4$/GO	RB-19 dye	Xe- lamp	80 ppm	0.6 g L^{-1}	60	99.0	139
Fe/GO/titanium phosphate	RhB	Two 500 W halogen lamps	10 ppm	50 mg	100	90	140
NCR	BG	UV lamp	10 ppm	50 mg	60	92	141
(PVA/PAAc)–RGO–TiO	DB71	UV light	40 ppm	200 mg	40	100	142
Ag/AgBr/rGO	RhB	Visible-light	1.0×10^{-5} M	25 mg	30	87	143
T0.05–100/Dia-GO	MB	Visible light	100 ppm	100 mg	300	78.37	119
	MR		100 ppm	100 mg	300	41.5	
	CR		100 ppm	100 mg	300	43.42	
ZnO–Bi_2O_3/GO	AB	Visible light	10 ppm	50 mg	120	98.31	144
	AY		10 ppm	50 mg	120	88.69	
	AR		10 ppm	50 mg	120	81.93	
	RB		10 ppm	50 mg	120	44.23	
	RY		10 ppm	50 mg	120	80.28	
	RR		10 ppm	50 mg	120	80.35	

[a] PANI/rGO, polyaniline/reduced graphene oxide composite; BG, Brilliant green; NCR, nickel/copper oxide/reduced graphene oxide; MG, malachite green; RhB, Rhodamine B; MB; methylene blue; MR, methyl red; CR, Congo red; T0.05–100/Dia-GO, titanium dioxide/diazonium/graphene oxide; (PVA/PAAc)–RGO–TiO, polyvinyl alcohol/acrylic polyvinyl alcohol/reduced graphene oxide/titanium dioxide; DB71, direct blue 71 dye; MO, Methyl orange; WO_3/graphene, tungsten trioxide nanorods–graphene nanostructure, AB25, Acid Blue 25; AgI/RGO, silver iodide/reduced graphene oxide; AB-BL, active black BL-G, AB, Acid Blue; AY, Acid Yellow; AR, Acid Red; RB, Reactive Blue, RY, Reactive Yellow; RR, Reactive Red; 2,4, DNP, 2,4-dintirophenol; TiO_2/Gr/30 PW, (30 wt% loading of 12- tungstophosphoric acid to TiO_2/Gr); BPA, bisphenol.

the dissociation of H_2O_2 and the formation of the highly reactive OH$^{\bullet}$ radicals, responsible for the dyes degradation. However, in basic conditions, the concentration of OH$^-$ ion increases and reacts with positively charged holes to form highly active OH$^{\bullet}$ radicals. The obtained results also suggested that the presence of H$^+$ or OH$^-$ ions significantly delayed the electron–hole recombination.[85]
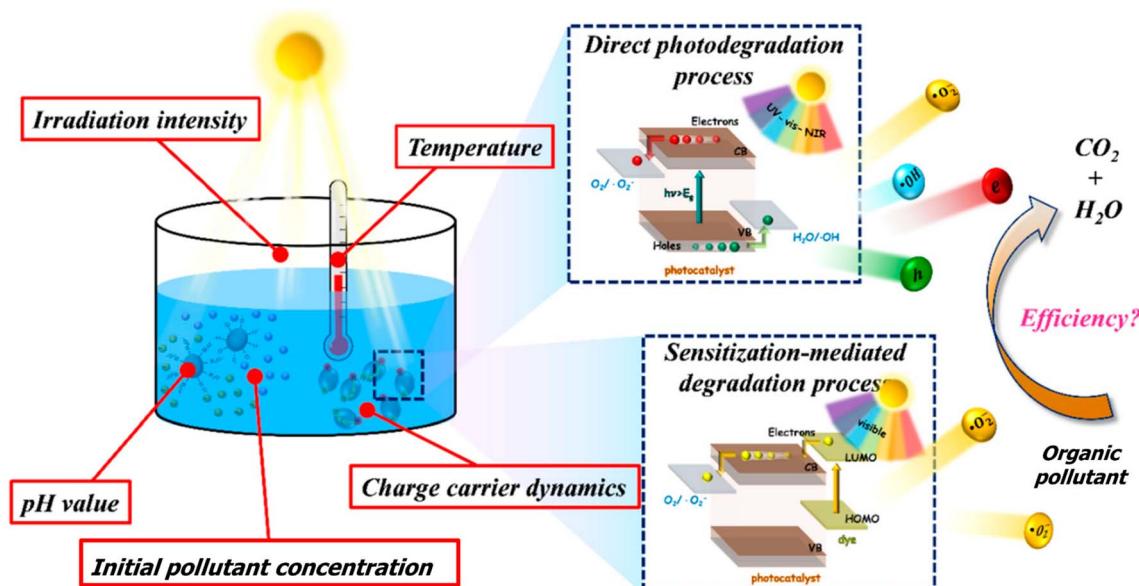
Fig. 10 Schematic shown of operational parameters affecting the photocatalytic degradation of organic pollutants.[81]
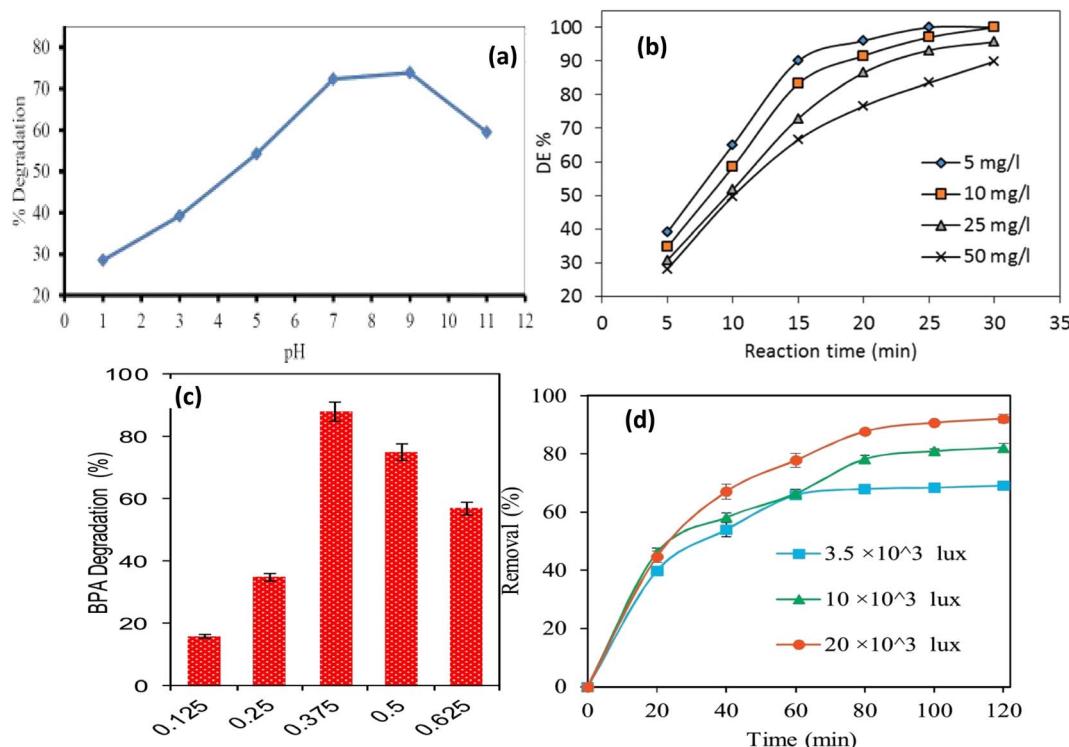
Fig. 11 Effects of operating parameters on degradation performance, (a) pH reprinted with permission from ref. 84, (b) initial concentration of pollutant reprinted with permission from ref. 88, (c) catalyst weigh, reprinted with permission from ref. 93, and (d) visible light intensity reprinted with permission from ref. 96. Copyright 2022 Elsevier.

4.1.1.2 Effect of initial pollutant concentration. The initial concentration of the organic pollutant significantly affects the photodegradation activity. Previous research found that increasing the initial concentration to a certain extent increased photo degradation; however, increasing the initial concentration further decreased photocatalytic activity due to the difficulty of light reaching the photocatalyst surfaces,[86] and surface adsorbed pollutant molecules prevent reactive radicals from interacting with the catalyst surfaces.[87] Thus, photo degradation decreased with higher initial pollutant concentration as part of the irradiation light is absorbed by the pollutant molecules and prevented from interacting with the catalyst surfaces,[88] Fig. 11b. Further, the decreased photocatalytic efficiency was also attributed to the limited generation of OH˙ radicals by the heavily covered photocatalyst surfaces.[89] Similarly, the reduced degradation efficiency at high initial concentrations of pollutants was attributed to the low penetration of light and limited availability of surface active sites of the photocatalyst.[90]

4.1.1.3 Effect of photocatalyst dose. Photocatalyst weight is a significant parameter in photocatalytic processes, wherein the increase in the photocatalyst mass provides more active sites and increases the generation of hydroxyl and peroxide radicals.[91] However, exceeding the optimum photocatalyst dosage can reduce photocatalytic activity due to catalyst particle agglomeration and the resulting decrease in active surface area, as well as irradiant light penetration.[92] Thus, increasing the catalyst mass increased the photocatalytic efficiency up to an optimum dose, after which increasing the catalyst mass

increased the turbidity of the test solution, which increased light scattering and inhibited photocatalytic pollutant degradation, Fig. 11c.[93,94] On the other hand, the rate of the malachite green dye degradation increased rapidly by increasing the catalyst dose and then remained almost constant in the range of 23.5–43.5 mg of the catalyst.[95]

4.1.1.4 Effect of irradiation light intensity. The excitation of photocatalysts is usually improved by raising the incident light intensity. At low light intensities, the separation of photogenerated electron–hole pairs suffers from recombination, which reduces the formation of free radicals and the degradation efficiency of organic pollutants; this effect can be overcome by increasing the light intensity. Thus, increasing the intensity of incident light increased the efficiency of pollutant degradation because more photons were present for excitation, resulting in the formation of more photogenerated pairs in the semiconductor and an increase in reaction rate, Fig. 11d.[96] Similar results were obtained by other works.[97,98]

4.1.1.5 Effect of oxidizing species. In photocatalytic reactions, oxygen species and reactive radicals are considered the main contributors to pollutant's degradation. Oxidants enhance the performance of the degradation process and decrease reaction time by the generation of reactive oxygen species.[99] For example, H_2O_2 can produce hydroxyl radicals and withdraw electrons away from the CB resulting in improvements in the separation of charge. However, excess H_2O_2 can act as a scavenger for OH˙ or produce peroxyl groups which may adversely effect the degradation process.[100] Thus, the addition of H_2O_2 reduced the

degradation time of crystal violet dye from 280 to 60 minutes; however, large amounts of H_2O_2 resulted in less effective $OH^{\cdot}$ radicals.[101] Further, the H_2O_2 dose exhibited a prominent effect on the degradation characteristics of MB on $FeVO_4$; where higher concentrations of H_2O_2 resulted in poor degradation due to recombination effects.[102] Similarly, in the presence of hydrogen peroxide and proper catalysts, azo dyes underwent rapid photocatalytic degradation.[103]

4.2 Hydrogen production

By 2050, the energy gap from conventional energy sources including natural gas, coal, and oil will be 14 TW, which requires the search for sustainable sources to bridge this gap.[104] Nature stores large amounts of hydrogen in the form of water. Therefore, the environmentally friendly production of hydrogen using the efficient combination of solar energy and water has significant potential to satisfy the world's energy demands nowadays as well as in the future. Several semiconductors have been used to catalyze the generation of hydrogen from water. The quick recombination of photogenerated electrons and holes within photocatalysts limits the practical applicability of this technique. The incorporation of graphene onto the semiconductor can improve photocatalytic H_2-production. For instance, $rGO/MoS_2/g-C_3N_4$ heterostructure photocatalyst was synthesized by hydrothermal route and showed a high H_2-production rate of 317 $\mu mol\ h^{-1}\ g^{-1}$, and a quantum yield of 3.4% at 420 nm.[105] The ternary photocatalyst exhibited greater photocatalytic activity compared to optimized Pt-loaded g-C_3N_4.[105] Further, incorporation of N-doped graphene onto CdS photocatalyst greatly improved the hydrogen generation rate, from solution containing Na_2S and Na_2SO under visible-light irradiation.[106] The reported optimal content of N-doped graphene was 2.0 wt%, which produced a H_2-generation rate of 210 $\mu mol\ h^{-1}$ compared to bare CdS that gave 40 $\mu mol\ h^{-1}$. The potential of graphene is lower than the CB of CdS and greater than the reduction potential of H^+, which facilitates the transport of electrons from the CB of CdS to graphene and the reduction of H^+, and consequently improves the H_2-production activity. Moreover, graphene/$AgIO_4$/ZnO/heterostructure was synthesized *via* a sonochemical route for the photoproduction of hydrogen.[107] The generation in $OH^{\cdot}$ radical (E_{VB} = +2.88 eV) that is recorded from PL analysis of terephthalic acid demonstrated charge migration that was dominant through the Z-scheme.[107]

5. Desorption and regeneration

Photocatalyst regeneration and recycling are regarded as essential basic elements of any photocatalytic process from an economic and environmental perspective. The regeneration and reuse of photocatalysts lower the operation cost, which is extremely desirable for real wastewater treatment plants. Several GO-semiconductor composites exhibited great reusability with most tested organic pollutants. For example, Fe_3O_4-amino functionalized GO exhibited a 97% removal efficiency of Reactive Black 5 after six cycles of reuse.[108] The reduction of

nearly 3% in the elimination efficiency can be related to the saturation of active sites of photocatalysts.[108] Further, the rGO-based photocatalyst was successfully used four consecutive cycles using acetone as the regenerating agent.[109] Moreover, XRD, FTIR, and SEM results did not display any significant chemical or morphological changes in ZnO/$CoFe_2O_4$/N-doped G and ZnO/$ZnFe_2O_4$/N-doped G photocatalysts after ten repeated cycles.[110] However, with $MnFe_2O_4$/rGO the photocatalytic degradation efficiency decreased slightly and reached 88% after the fourth run.[77]

6. Conclusions and perspectives

In this study, we reviewed various strategies for the synthesis and characterization of semiconductors/graphene-based photocatalysts and their potential applications in photocatalytic H_2-production as well as degradation of organic pollutants, *e.g.*, dyes, pharmaceuticals, phenols and pesticides. The incorporation of graphene or one of its derivatives into semiconductors significantly boost the photocatalytic performance by enhancing the adsorption ability, and light harvesting in the visible domain, and reducing the band-gap energy as well as by inhibiting the recombination of the photogenerated electron–hole pairs. Studies of various parameters affecting photocatalytic processes revealed that increasing the oxidant dose, catalyst mass, and irradiation time up to a certain optimum limit generally improved the rate of photocatalytic degradation, while increasing the initial pollutant concentration generally decreased it. The pH of the solution, on the other hand, can have a dual impact on the process. The mechanisms of the photocatalytic process have been thoroughly discussed. The reusability studies revealed the high efficiency of graphene-based photocatalysts. However, there are more research gaps and challenges that need to be addressed and studied in detail in the future:

(1) Designing the morphology of graphene/semiconductor composite to further enhancement of the photocatalytic performance. Materials designing should aim at improved light harvesting, increased catalyst surface area, and enhanced mass transport.

(2) Many studies dealt with improving the performance of photocatalysis over short periods of time and under optimal experimental conditions. The performance of the catalysts should be tested over long periods to study their stability and simulated wastewater should be utilized for photocatalytic experiments.

(3) The majority of photocatalytic experiments are carried out on a laboratory scale, but future work should concentrate on the efficiency of the prepared photocatalyst on a pilot scale to validate their effectiveness in industrial applications and identify the real operational challenges. The economic feasibility and return on investment of using these materials in various applications should also be investigated.

(4) Finally, the bio-safety of composites must be emphasized. When used in wastewater remediation, a portion of the synthesized composite may be released into the environment.

Following that, the full extent of these composites' toxicity to humans, animals, and the environment must be investigated.

Despite the challenges mentioned, graphene-based semiconductor photocatalysts have limitless applications and prospects in solving energy shortages and industrial waste treatment.

Conflicts of interest

Authors declare no conflict of interest.

References

1 M. Adel, M. A. Ahmed and A. A. Mohamed, Effective removal of indigo carmine dye from wastewaters by adsorption onto mesoporous magnesium ferrite nanoparticles, *Environ. Nanotechnol., Monit. Manage.*, 2021, **16**, 100550.

2 M. Adel, *et al.*, Characterization of fouling for a full-scale seawater reverse osmosis plant on the Mediterranean sea: Membrane autopsy and chemical cleaning efficiency, *Groundwater for Sustainable Development*, 2022, 16, p. 100704.

3 G. Ramalingam, *et al.*, A review of graphene-based semiconductors for photocatalytic degradation of pollutants in wastewater, *Chemosphere*, 2022, 134391.

4 Q. Liang, *et al.*, Construction of fish-scale tubular carbon nitride-based heterojunction with boosting charge separation in photocatalytic tetracycline degradation and H_2O_2 production, *Chem. Eng. J.*, 2021, **426**, 130831.

5 T. Wu, *et al.*, Construction of a novel S-scheme heterojunction piezoelectric photocatalyst V-BiOIO$_3$/FTCN and immobilization with floatability for tetracycline degradation, *J. Hazard. Mater.*, 2023, **443**, 130251.

6 M. A. Ahmed, M. A. Ahmed and A. A. Mohamed, Facile adsorptive removal of dyes and heavy metals from wastewaters using magnetic nanocomposite of zinc ferrite@ reduced graphene oxide, *Inorg. Chem. Commun.*, 2022, **144**, 109912.

7 M. A. Ahmed and A. A. Mohamed, A systematic review of layered double hydroxide-based materials for environmental remediation of heavy metals and dye pollutants, *Inorg. Chem. Commun.*, 2023, **148**, 110325.

8 M. Adel, *et al.*, Removal of heavy metals and dyes from wastewater using graphene oxide-based nanomaterials: A critical review, *Environ. Nanotechnol., Monit. Manage.*, 2022, **18**, 100719.

9 M. Adel, M. A. Ahmed and A. A. Mohamed, Effective removal of cationic dyes from aqueous solutions using reduced graphene oxide functionalized with manganese ferrite nanoparticles, *Compos. Commun.*, 2020, **22**, 100450.

10 M. Adel, M. A. Ahmed and A. A. Mohamed, Synthesis and characterization of magnetically separable and recyclable crumbled MgFe$_2$O$_4$/reduced graphene oxide nanoparticles for removal of methylene blue dye from aqueous solutions, *J. Phys. Chem. Solids*, 2021, **149**, 109760.

11 J. Barasarathi, P. S. Abdullah and E. C. Uche, Application of magnetic carbon nanocomposite from agro-waste for the removal of pollutants from water and wastewater, *Chemosphere*, 2022, 135384.

12 R. K. Bastian, P. E. Shanaghan, and B. P. Thompson, Use of wetlands for municipal wastewater treatment and disposal–Regulatory issues and EPA policies, *Constructed Wetlands for Wastewater Treatment*, 2020, pp. 265–278.

13 T. Wu, *et al.*, Hydrogen peroxide-impregnated supramolecular precursors synthesize mesoporous-rich ant nest-like filled tubular g-C$_3$N$_4$ for effective photocatalytic removal of pollutants, *Chem. Eng. J.*, 2022, 137332.

14 H. F. G. Mejía, *et al.*, Direct recycling of discarded reverse osmosis membranes for domestic wastewater treatment with a focus on water reuse, *Chem. Eng. Res. Des.*, 2022, **184**, 473–487.

15 K. Q. Jabbar, A. A. Barzinjy and S. M. Hamad, Iron oxide nanoparticles: Preparation methods, functions, adsorption and coagulation/flocculation in wastewater treatment, *Environ. Nanotechnol., Monit. Manage.*, 2022, **17**, 100661.

16 S. Patial, *et al.*, Recent advances in photocatalytic multivariate metal organic frameworks-based nanostructures toward renewable energy and the removal of environmental pollutants, *Mater. Today Energy*, 2021, **19**, 100589.

17 H. Lu, *et al.*, A high-performance Bi$_2$O$_3$/Bi$_2$SiO$_5$ pn heterojunction photocatalyst induced by phase transition of Bi$_2$O$_3$, *Appl. Catal., B*, 2018, **237**, 59–67.

18 L. Yang, *et al.*, Beyond C$_3$N$_4$ π-conjugated metal-free polymeric semiconductors for photocatalytic chemical transformations, *Chem. Soc. Rev.*, 2021, **50**(3), 2147–2172.

19 X. Li, *et al.*, A "bottle-around-ship" like method synthesized yolk-shell Ag$_3$PO$_4$@ MIL-53 (Fe) Z-scheme photocatalysts for enhanced tetracycline removal, *J. Colloid Interface Sci.*, 2020, **561**, 501–511.

20 S. Dong, *et al.*, A novel and high-performance double Z-scheme photocatalyst ZnO-SnO$_2$-Zn$_2$SnO$_4$ for effective removal of the biological toxicity of antibiotics, *J. Hazard. Mater.*, 2020, **399**, 123017.

21 Q. Liang, *et al.*, Recent advances of melamine self-assembled graphitic carbon nitride-based materials: design, synthesis and application in energy and environment, *Chem. Eng. J.*, 2021, **405**, 126951.

22 X. Zhang, *et al.*, Recent advances of Zr based metal organic frameworks photocatalysis: Energy production and environmental remediation, *Coord. Chem. Rev.*, 2021, **448**, 214177.

23 L. Ji, *et al.*, Enhanced visible-light-induced photocatalytic disinfection of Escherichia coli by ternary Bi$_2$WO$_6$/TiO$_2$/reduced graphene oxide composite materials: Insight into the underlying mechanism, *Adv. Powder Technol.*, 2020, **31**(1), 128–138.

24 D. Ramírez-Ortega, *et al.*, Enhancing the photocatalytic hydrogen production of the ZnO–TiO$_2$ heterojunction by supporting nanoscale Au islands, *Int. J. Hydrogen Energy*, 2021, **46**(69), 34333–34343.

25 M. Al Kausor and D. Chakrabortty, Facile fabrication of N-TiO$_2$/Ag$_3$PO$_4$@ GO nanocomposite toward photodegradation of organic dye under visible light, *Inorg. Chem. Commun.*, 2020, **116**, 107907.

26 M. Al Kausor, S. S. Gupta and D. Chakrabortty, Ag$_3$PO$_4$-based nanocomposites and their applications in photodegradation of toxic organic dye contaminated wastewater: review on material design to performance enhancement, *J. Saudi Chem. Soc.*, 2020, **24**(1), 20–41.

27 M. Al Kausor and D. Chakrabortty, Graphene oxide based semiconductor photocatalysts for degradation of organic dye in waste water: a review on fabrication, performance enhancement and challenges, *Inorg. Chem. Commun.*, 2021, **129**, 108630.

28 W. Wang, *et al.*, Sulfur doped carbon quantum dots loaded hollow tubular g-C$_3$N$_4$ as novel photocatalyst for destruction of Escherichia coli and tetracycline degradation under visible light, *Chem. Eng. J.*, 2019, **378**, 122132.

29 Y. Chen, *et al.*, Hybrid photocatalysts using semiconductor/MOF/graphene oxide for superior photodegradation of organic pollutants under visible light, *Mater. Sci. Semicond. Process.*, 2020, **107**, 104838.

30 M. Adel, M. A. Ahmed and A. A. Mohamed, A facile and rapid removal of cationic dyes using hierarchically porous reduced graphene oxide decorated with manganese ferrite, *FlatChem*, 2021, **26**, 100233.

31 A. A. Balandin, Thermal properties of graphene and nanostructured carbon materials, *Nat. Mater.*, 2011, **10**(8), 569–581.

32 K. I. Bolotin, *et al.*, Ultrahigh electron mobility in suspended graphene, *Solid State Commun.*, 2008, **146**(9–10), 351–355.

33 Y. Zhu, *et al.*, Graphene and graphene oxide: synthesis, properties, and applications, *Adv. Mater.*, 2010, **22**(35), 3906–3924.

34 D. Chen, H. Feng and J. Li, Graphene oxide: preparation, functionalization, and electrochemical applications, *Chem. Rev.*, 2012, **112**(11), 6027–6053.

35 F. Li, *et al.*, Graphene oxide: A promising nanomaterial for energy and environmental applications, *Nano energy*, 2015, **16**, 488–515.

36 D. Luo and X. Zhang, The effect of oxygen–containing functional groups on the H$_2$ adsorption of graphene–based nanomaterials: experiment and theory, *Int. J. Hydrogen Energy*, 2018, **43**(11), 5668–5679.

37 D. P. Kumar, *et al.*, Ultrathin MoS$_2$ layers anchored exfoliated reduced graphene oxide nanosheet hybrid as a highly efficient cocatalyst for CdS nanorods towards enhanced photocatalytic hydrogen production, *Appl. Catal., B*, 2017, **212**, 7–14.

38 F. Chen, *et al.*, Highly efficient removal of bisphenol A by a three-dimensional graphene hydrogel-AgBr@ rGO exhibiting adsorption/photocatalysis synergy, *Appl. Catal., B*, 2017, **217**, 65–80.

39 S. Bibi, *et al.*, Photocatalytic degradation of malachite green and methylene blue over reduced graphene oxide (rGO) based metal oxides (rGO–Fe$_3$O$_4$/TiO$_2$) nanocomposite under UV-visible light irradiation, *J. Environ. Chem. Eng.*, 2021, **9**(4), 105580.

40 Y. J. Lee and Y. Park, Graphene oxide grafted gold nanoparticles and silver/silver chloride nanoparticles green-synthesized by a Portulaca oleracea extract: Assessment of catalytic activity, *Colloids Surf., A*, 2020, **607**, 125527.

41 Y.-H. Chen, B.-K. Wang and W.-C. Hou, Graphitic carbon nitride embedded with graphene materials towards photocatalysis of bisphenol A: The role of graphene and mediation of superoxide and singlet oxygen, *Chemosphere*, 2021, **278**, 130334.

42 S. Chowdhury and R. Balasubramanian, Graphene/semiconductor nanocomposites (GSNs) for heterogeneous photocatalytic decolorization of wastewaters contaminated with synthetic dyes: a review, *Appl. Catal., B*, 2014, **160**, 307–324.

43 H. Wang, *et al.*, Nanocrystal growth on graphene with various degrees of oxidation, *J. Am. Chem. Soc.*, 2010, **132**(10), 3270–3271.

44 L. Wang, *et al.*, In-situ growth of few-layer graphene on ZnO with intimate interfacial contact for enhanced photocatalytic CO$_2$ reduction activity, *Chem. Eng. J.*, 2021, **411**, 128501.

45 C. Han, N. Zhang and Y.-J. Xu, Structural diversity of graphene materials and their multifarious roles in heterogeneous photocatalysis, *Nano Today*, 2016, **11**(3), 351–372.

46 X. Huang, *et al.*, Graphene-based composites, *Chem. Soc. Rev.*, 2012, **41**(2), 666–686.

47 V. Singh, *et al.*, Graphene based materials: past, present and future, *Prog. Mater. Sci.*, 2011, **56**(8), 1178–1271.

48 I. Altin, *et al.*, Hydrothermal preparation of B–TiO$_2$-graphene oxide ternary nanocomposite, characterization and photocatalytic degradation of bisphenol A under simulated solar irradiation, *Mater. Sci. Semicond. Process.*, 2021, **123**, 105591.

49 K. P. Mubiayi, *et al.*, Microwave assisted synthesis of CuInGaSe$_2$ quantum dots and spray deposition of their composites with graphene oxide derivatives, *Mater. Chem. Phys.*, 2020, **242**, 122449.

50 A. Velasco-Hernández, *et al.*, Synthesis and characterization of graphene oxide-TiO$_2$ thin films by sol-gel for photocatalytic applications, *Mater. Sci. Semicond. Process.*, 2020, **114**, 105082.

51 B. Bashir, *et al.*, Cu$_x$Ni1-xO nanostructures and their nanocomposites with reduced graphene oxide: Synthesis, characterization, and photocatalytic applications, *Ceram. Int.*, 2021, **47**(3), 3603–3613.

52 L. Meng, Y. Qu and L. Jing, Recent advances in BiOBr-based photocatalysts for environmental remediation, *Chin. Chem. Lett.*, 2021, **32**(11), 3265–3276.

53 A. M. Hamza and Q. A. Yousif, Facile one-pot solvothermal technique to synthesis ZnS/graphene nanoplatelets (0.2) nanocomposites, *J. Phys.: Conf. Ser.*, 2020, **1664**, 012055.

54 L. Sun, et al., Solvothermal fabrication and enhanced visible light photocatalytic activity of Cu_2O-reduced graphene oxide composite microspheres for photodegradation of Rhodamine B, Appl. Surf. Sci., 2015, 358, 91–99.

55 G. Vinodhkumar, et al., Solvothermal synthesis of magnetically separable reduced graphene oxide/Fe_3O_4 hybrid nanocomposites with enhanced photocatalytic properties, Phys. B, 2020, 580, 411752.

56 V. L. Siong, et al., One-step solvothermal synthesis of rGO/TiO_2 nanocomposite for efficient solar photocatalytic degradation of methylene blue dye, Curr. Nanosci., 2019, 15(2), 157–162.

57 Q. Li, et al., Highly efficient visible-light-driven photocatalytic hydrogen production of CdS-cluster-decorated graphene nanosheets, J. Am. Chem. Soc., 2011, 133(28), 10878–10884.

58 M. Mohammadi, et al., Boehmite nanoparticles as versatile support for organic–inorganic hybrid materials: Synthesis, functionalization, and applications in eco-friendly catalysis, J. Ind. Eng. Chem., 2021, 97, 1–78.

59 M. Azarang, et al., Effects of graphene oxide concentration on optical properties of ZnO/RGO nanocomposites and their application to photocurrent generation, J. Appl. Phys., 2014, 116(8), 084307.

60 K. Li, et al., Simulated sunlight photodegradation of aqueous atrazine and Rhodamine B catalyzed by the ordered mesoporous graphene–titania/silica composite material, Catal. Commun., 2012, 18, 16–20.

61 D. Xu, et al., Noble metal-free RGO/TiO_2 composite nanofiber with enhanced photocatalytic H_2-production performance, Appl. Surf. Sci., 2018, 434, 620–625.

62 Y. Yang, et al., Green and facile microwave-assisted synthesis of TiO_2/graphene nanocomposite and their photocatalytic activity for methylene blue degradation, Russ. J. Phys. Chem. A, 2014, 88(3), 478–483.

63 R. Kumar, et al., Microwave heating time dependent synthesis of various dimensional graphene oxide supported hierarchical ZnO nanostructures and its photoluminescence studies, Mater. Des., 2016, 111, 291–300.

64 H. Hu, et al., Rapid microwave-assisted synthesis of graphene nanosheets–zinc sulfide nanocomposites: Optical and photocatalytic properties, Synth. Met., 2011, 161(5–6), 404–410.

65 S. Prabhu, et al., Synthesis, structural and optical properties of ZnO spindle/reduced graphene oxide composites with enhanced photocatalytic activity under visible light irradiation, Opt. Mater., 2018, 79, 186–195.

66 J. Guo, et al., Sonochemical synthesis of TiO_2 nanoparticles on graphene for use as photocatalyst, Ultrason. Sonochem., 2011, 18(5), 1082–1090.

67 J. Liu, et al., Gram-scale production of graphene oxide–TiO_2 nanorod composites: towards high-activity photocatalytic materials, Appl. Catal., B, 2011, 106(1–2), 76–82.

68 X. Liua, et al., Changqing Sunc UV-assisted photocatalytic synthesis of ZnO–reduced graphene oxide composites with enhanced photocatalytic activity in reduction of Cr (VI), Chem. Eng. J., 2012, 183, 238–243.

69 T. Mahvelati-Shamsabadi, et al., ZnS@ reduced graphene oxide nanocomposite as an effective sunlight driven photocatalyst for degradation of reactive black 5: a mechanistic approach, Sep. Purif. Technol., 2018, 202, 326–334.

70 J. Choi, et al., Green synthesis of the reduced graphene oxide–CuI quasi-shell–core nanocomposite: a highly efficient and stable solar-light-induced catalyst for organic dye degradation in water, Appl. Surf. Sci., 2015, 358, 159–167.

71 T. Govindaraj, et al., Fabrication of WO_3 nanorods/RGO hybrid nanostructures for enhanced visible-light-driven photocatalytic degradation of Ciprofloxacin and Rhodamine B in an ecosystem, J. Alloys Compd., 2021, 868, 159091.

72 X. An, et al., One-pot synthesis of In_2S_3 nanosheets/graphene composites with enhanced visible-light photocatalytic activity, Appl. Catal., B, 2013, 129, 80–88.

73 S. Muninathan and S. Arumugam, Enhanced photocatalytic activities of NiS decorated reduced graphene oxide for hydrogen production and toxic dye degradation under visible light irradiation, Int. J. Hydrogen Energy, 2021, 46(9), 6532–6546.

74 A. Iwase, et al., Reduced graphene oxide as a solid-state electron mediator in Z-scheme photocatalytic water splitting under visible light, J. Am. Chem. Soc., 2011, 133(29), 11054–11057.

75 E. György, et al., Enhanced UV-and visible-light driven photocatalytic performances and recycling properties of graphene oxide/ZnO hybrid layers, Ceram. Int., 2018, 44(2), 1826–1835.

76 M. A. E. Wafi, et al., Exceptional removal of methylene blue and p-aminophenol dye over novel TiO_2/RGO nanocomposites by tandem adsorption-photocatalytic processes, Mater. Sci. Energy Technol., 2022, 5, 217–231.

77 B. Mandal, et al., $MnFe_2O_4$ decorated reduced graphene oxide heterostructures: nanophotocatalyst for methylene blue dye degradation, Vacuum, 2020, 173, 109150.

78 P. Makal and D. Das, Superior photocatalytic dye degradation under visible light by reduced graphene oxide laminated TiO_2-B nanowire composite, J. Environ. Chem. Eng., 2019, 7(5), 103358.

79 H. H. Mohamed, Rationally designed Fe_2O_3/GO/WO3 Z-Scheme photocatalyst for enhanced solar light photocatalytic water remediation, J. Photochem. Photobiol., A, 2019, 378, 74–84.

80 J. Ding, et al., Low-temperature preparation of magnetically separable Fe_3O_4@ CuO-RGO core-shell heterojunctions for high-performance removal of organic dye under visible light, J. Alloys Compd., 2016, 688, 649–656.

81 Y.-H. Chiu, et al., Mechanistic insights into photodegradation of organic dyes using heterostructure photocatalysts, Catalysts, 2019, 9(5), 430.

82 H. A. A. Jamjoum, *et al.*, Synthesis, characterization, and photocatalytic activities of graphene oxide/metal oxides nanocomposites: A review, *Front. Chem.*, 2021, **9**, 752276.

83 Á. Pérez-Molina, *et al.*, Functionalized graphene derivatives and TiO$_2$ for high visible light photodegradation of azo dyes, *Nanomaterials*, 2020, **10**(6), 1106.

84 P. Nuengmatcha, *et al.*, Sonocatalytic performance of ZnO/graphene/TiO$_2$ nanocomposite for degradation of dye pollutants (methylene blue, texbrite BAC-L, texbrite BBU-L and texbrite NFW-L) under ultrasonic irradiation, *Dyes Pigm.*, 2016, **134**, 487–497.

85 J. Varghese, CuS–ZnS decorated graphene nanocomposites: Synthesis and photocatalytic properties, *J. Phys. Chem. Solids*, 2021, **156**, 109911.

86 K. M. Reza, A. Kurny and F. Gulshan, Parameters affecting the photocatalytic degradation of dyes using TiO$_2$: a review, *Appl. Water Sci.*, 2017, **7**(4), 1569–1578.

87 N. Daneshvar, D. Salari and A. Khataee, Photocatalytic degradation of azo dye acid red 14 in water on ZnO as an alternative catalyst to TiO$_2$, *J. Photochem. Photobiol., A*, 2004, **162**(2–3), 317–322.

88 T. J. Al-Musawi, *et al.*, Development of sonophotocatalytic process for degradation of acid orange 7 dye by using titanium dioxide nanoparticles/graphene oxide nanocomposite as a catalyst, *J. Environ. Manage.*, 2021, **292**, 112777.

89 M. Iqbal, *et al.*, Graphene oxide nanocomposite with CuSe and photocatalytic removal of methyl green dye under visible light irradiation, *Diamond Relat. Mater.*, 2021, **113**, 108254.

90 H. Alijani, M. Abdouss and H. Khataei, Efficient photocatalytic degradation of toxic dyes over BiFeO$_3$/CdS/rGO nanocomposite under visible light irradiation, *Diamond Relat. Mater.*, 2022, **122**, 108817.

91 M. S. Nasrollahzadeh, *et al.*, Synthesis of ZnO nanostructure using activated carbon for photocatalytic degradation of methyl orange from aqueous solutions, *Appl. Water Sci.*, 2018, **8**(4), 1–12.

92 I. Khan, *et al.*, Heterogeneous photodegradation of industrial dyes: an insight to different mechanisms and rate affecting parameters, *J. Environ. Chem. Eng.*, 2020, **8**(5), 104364.

93 N. Hassan, *et al.*, Photodegradation of bisphenol A from aqueous solution over reduced graphene oxide supported on tetragonal silica-zirconia nanocatalysts: Optimization using RSM, *Process Saf. Environ. Prot.*, 2021, **156**, 496–507.

94 T. Q. Q. Viet, *et al.*, Enhanced photodegradation toward graphene–based MgFe$_2$O$_4$–TiO$_2$: Investigation and optimization, *Int. J. Hydrogen Energy*, 2022, **47**(75), 32092–32106.

95 N. Zada, I. Khan and K. Saeed, Synthesis of multiwalled carbon nanotubes supported manganese and cobalt zinc oxides nanoparticles for the photodegradation of malachite green, *Sep. Sci. Technol.*, 2017, **52**(8), 1477–1485.

96 S. Dehghan, *et al.*, Visible-light-driven photocatalytic degradation of Metalaxyl by reduced graphene oxide/Fe$_3$O$_4$/ZnO ternary nanohybrid: Influential factors,

mechanism and toxicity bioassay, *J. Photochem. Photobiol., A*, 2019, **375**, 280–292.

97 I. Ahmad, Q. Fasihullah and F. H. Vaid, Effect of light intensity and wavelengths on photodegradation reactions of riboflavin in aqueous solution, *J. Photochem. Photobiol., B*, 2006, **82**(1), 21–27.

98 F. Hussin, *et al.*, Photocatalytic synthesis of reduced graphene oxide–zinc oxide: effects of light intensity and exposure time, *J. Photochem. Photobiol., A*, 2017, **340**, 128–135.

99 D. Wu, *et al.*, Rapid removal of azophloxine via catalytic degradation by a novel heterogeneous catalyst under visible light, *Catalysts*, 2020, **10**(1), 138.

100 N. Pathak, *et al.*, Photocatalytic and photochemical oxidation of ethylene: Potential for storage of fresh produce—A review, *Food Bioprocess Technol.*, 2017, **10**(6), 982–1001.

101 M. Rahmat, *et al.*, Highly efficient removal of crystal violet dye from water by MnO$_2$ based nanofibrous mesh/photocatalytic process, *J. Mater. Res. Technol.*, 2019, **8**(6), 5149–5159.

102 M. M. Sajid, *et al.*, Photocatalytic performance of ferric vanadate (FeVO$_4$) nanoparticles synthesized by hydrothermal method, *Mater. Sci. Semicond. Process.*, 2021, **129**, 105785.

103 M. Ashraf, *et al.*, Hematite and magnetite nanostructures for green and sustainable energy harnessing and environmental pollution control: a review, *Chem. Res. Toxicol.*, 2019, **33**(6), 1292–1311.

104 C. Prasad, *et al.*, An overview of graphene oxide supported semiconductors based photocatalysts: Properties, synthesis and photocatalytic applications, *J. Mol. Liq.*, 2020, **297**, 111826.

105 Y.-J. Yuan, *et al.*, Promoting charge separation in g-C$_3$N$_4$/graphene/MoS$_2$ photocatalysts by two-dimensional nanojunction for enhanced photocatalytic H$_2$ production, *ACS Appl. Energy Mater.*, 2018, **1**(4), 1400–1407.

106 L. Jia, *et al.*, Highly durable N-doped graphene/CdS nanocomposites with enhanced photocatalytic hydrogen evolution from water under visible light irradiation, *J. Phys. Chem. C*, 2011, **115**(23), 11466–11473.

107 A. Galal, M. G. Elmahgary and M. Ahmed, Construction of novel AgIO$_4$/ZnO/graphene direct Z-scheme heterojunctions for exceptional photocatalytic hydrogen gas production, *Nanotechnol. Environ. Eng.*, 2021, **6**(1), 1–10.

108 M. P. da Silva, *et al.*, Photodegradation of Reactive Black 5 and raw textile wastewater by heterogeneous photo-Fenton reaction using amino-Fe$_3$O$_4$-functionalized graphene oxide as nanocatalyst, *Environ. Adv.*, 2021, **4**, 100064.

109 P. Sreelekshmi, R. R. Pillai and A. Meera, Controlled Synthesis of Novel Graphene Oxide Nanoparticles for the Photodegradation of Organic Dyes, *Top. Catal.*, 2022, 1–10.

110 N. Chandel, *et al.*, Magnetically separable ZnO/ZnFe$_2$O$_4$ and ZnO/CoFe2O4 photocatalysts supported onto nitrogen doped graphene for photocatalytic degradation of toxic dyes, *Arabian J. Chem.*, 2020, **13**(2), 4324–4340.

111 L. Chen, *et al.*, Three-dimensional titanium dioxide/ graphene hybrids with improved performance for photocatalysis and energy storage, *J. Colloid Interface Sci.*, 2018, **512**, 647–656.

112 D. A. Reddy, *et al.*, Green synthesis of AgI-reduced graphene oxide nanocomposites: toward enhanced visible-light photocatalytic activity for organic dye removal, *Appl. Surf. Sci.*, 2015, **341**, 175–184.

113 Y. Fu, *et al.*, Combination of cobalt ferrite and graphene: high-performance and recyclable visible-light photocatalysis, *Appl. Catal., B*, 2012, **111**, 280–287.

114 Y. Fu, X. Sun and X. Wang, BiVO₄–graphene catalyst and its high photocatalytic performance under visible light irradiation, *Mater. Chem. Phys.*, 2011, **131**(1–2), 325–330.

115 Z. Gao, *et al.*, Graphene–CdS composite, synthesis and enhanced photocatalytic activity, *Appl. Surf. Sci.*, 2012, **258**(7), 2473–2478.

116 M. Mitra, *et al.*, Polyaniline/reduced graphene oxide composite-enhanced visible-light-driven photocatalytic activity for the degradation of organic dyes, *ACS Omega*, 2019, **4**(1), 1623–1635.

117 M. A. Kausor and D. Chakrabortty, Optimization of system parameters and kinetic study of photocatalytic degradation of toxic acid blue 25 dye by Ag₃PO₄@ RGO nanocomposite, *J. Nanopart. Res.*, 2020, **22**(4), 1–17.

118 M. E. Khan, M. M. Khan and M. H. Cho, Fabrication of WO₃ nanorods on graphene nanosheets for improved visible light-induced photocapacitive and photocatalytic performance, *RSC Adv.*, 2016, **6**(25), 20824–20833.

119 N. T. V. Hoan, *et al.*, TiO₂/diazonium/graphene oxide composites: synthesis and visible-light-driven photocatalytic degradation of methylene blue, *J. Nanomater.*, 2020, **2020**, 4350125.

120 Y. Chen, *et al.*, Photochemical fabrication of SnO₂ dense layers on reduced graphene oxide sheets for application in photocatalytic degradation of p-Nitrophenol, *Appl. Catal., B*, 2017, **215**, 8–17.

121 D. K. Padhi, *et al.*, Green synthesis of Fe₃O₄/RGO nanocomposite with enhanced photocatalytic performance for Cr (VI) reduction, phenol degradation, and antibacterial activity, *ACS Sustainable Chem. Eng.*, 2017, **5**(11), 10551–10562.

122 E. Rafiee, *et al.*, Photocatalytic degradation of phenol using a new developed TiO₂/graphene/heteropoly acid nanocomposite: synthesis, characterization and process optimization, *RSC Adv.*, 2016, **6**(99), 96554–96562.

123 S. Mansingh, *et al.*, Pyrochlore Ce₂Zr₂O₇ decorated over rGO: a photocatalyst that proves to be efficient towards the reduction of 4-nitrophenol and degradation of ciprofloxacin under visible light, *Phys. Chem. Chem. Phys.*, 2018, **20**(15), 9872–9885.

124 A. Khataee, *et al.*, Fabrication of NiFe layered double hydroxide/reduced graphene oxide (NiFe-LDH/rGO) nanocomposite with enhanced sonophotocatalytic activity for the degradation of moxifloxacin, *Chem. Eng. J.*, 2019, **375**, 122102.

125 C. Mu, *et al.*, Removal of bisphenol A over a separation free 3D Ag₃PO₄–graphene hydrogel via an adsorption-photocatalysis synergy, *Appl. Catal., B*, 2017, **212**, 41–49.

126 Y. Li, *et al.*, Reduced graphene oxide three-dimensionally wrapped WO₃ hierarchical nanostructures as high-performance solar photocatalytic materials, *Appl. Catal., A*, 2016, **522**, 90–100.

127 S. Dong, *et al.*, ZnSnO₃ hollow nanospheres/reduced graphene oxide nanocomposites as high-performance photocatalysts for degradation of metronidazole, *Appl. Catal., B*, 2014, **144**, 386–393.

128 Y. Tang, *et al.*, Enhanced photocatalytic removal of tetrabromobisphenol A by magnetic CoO@ graphene nanocomposites under visible-light irradiation, *J. Mater. Res. Technol.*, 2018, **1**(6), 2698–2708.

129 J. Yang, *et al.*, BiVO₄ quantum tubes loaded on reduced graphene oxide aerogel as efficient photocatalyst for gaseous formaldehyde degradation, *Carbon*, 2018, **138**, 118–124.

130 N. Lu, *et al.*, Construction of Z-Scheme g-C₃N₄/RGO/WO₃ with in situ photoreduced graphene oxide as electron mediator for efficient photocatalytic degradation of ciprofloxacin, *Chemosphere*, 2019, **215**, 444–453.

131 P. Singh, *et al.*, Photocatalytic performance and quick recovery of BiOI/Fe₃O₄@ graphene oxide ternary photocatalyst for photodegradation of 2, 4-dinitrophenol under visible light, *Mater. Today Chem.*, 2019, **12**, 85–95.

132 X. Wang, A. Wang and J. Ma, Visible-light-driven photocatalytic removal of antibiotics by newly designed C₃N₄@ MnFe₂O₄–graphene nanocomposites, *J. Hazard. Mater.*, 2017, **336**, 81–92.

133 N. Hassan, *et al.*, Role of reduced graphene oxide in improving interfacial charge transfer of hybridized rGO/ silica/zirconia for enhanced Bisphenol A photodegradation, *J. Alloys Compd.*, 2019, **789**, 221–230.

134 Y. Yu, *et al.*, Mechanistic insights into TiO₂ thickness in Fe₃O₄@ TiO₂-GO composites for enrofloxacin photodegradation, *Chem. Eng. J.*, 2017, **325**, 647–654.

135 J. Ni, *et al.*, Construction of magnetically separable NiAl LDH/Fe₃O₄–RGO nanocomposites with enhanced photocatalytic performance under visible light, *Phys. Chem. Chem. Phys.*, 2018, **20**(1), 414–421.

136 Q. Wei, *et al.*, Construction of rGO wrapping octahedral Ag–Cu₂O heterostructure for enhanced visible light photocatalytic activity, *Appl. Catal., B*, 2018, **227**, 132–144.

137 F. Chen, *et al.*, Fabricating 3D porous PANI/TiO₂–graphene hydrogel for the enhanced UV-light photocatalytic degradation of BPA, *Appl. Surf. Sci.*, 2018, **427**, 123–132.

138 J. Kaur and M. Kaur, Facile fabrication of ternary nanocomposite of MgFe₂O₄·TiO₂@ GO for synergistic adsorption and photocatalytic degradation studies, *Ceram. Int.*, 2019, **45**(7), 8646–8659.

139 Y. Wang, *et al.*, Fabrication of BiVO₄/BiPO₄/GO composite photocatalytic material for the visible light-driven degradation, *J. Cleaner Prod.*, 2020, **247**, 119108.

140 N. A. Nahyoon, *et al.*, Significant photocatalytic degradation and electricity generation in the photocatalytic fuel cell

(PFC) using novel anodic nanocomposite of Fe, graphene oxide, and titanium phosphate, *Electrochim. Acta*, 2018, **271**, 41–48.

141 G. S. Sree, *et al.*, Enhanced UV–Visible triggered photocatalytic degradation of Brilliant green by reduced graphene oxide based NiO and CuO ternary nanocomposite and their antimicrobial activity, *Arabian J. Chem.*, 2020, **13**(4), 5137–5150.

142 M. F. Elshahawy, *et al.*, Fabrication of TiO_2 reduced graphene oxide based nanocomposites for effective of

photocatalytic decolorization of dye effluent, *J. Inorg. Organomet. Polym. Mater.*, 2020, **30**(7), 2720–2735.

143 X.-h. Meng, *et al.*, Ag/AgBr/rGO nanocomposite: Synthesis and its application in photocatalysis, *Mater. Lett.*, 2013, **105**, 162–165.

144 G. He, *et al.*, $ZnO–Bi_2O_3$/graphene oxide photocatalyst with high photocatalytic performance under visible light, *Mater. Technol.*, 2012, **27**(4), 278–283.